Vibrational dynamics of bond-center hydrogen in crystalline silicon

M. Budde,[1,*] C. Parks Cheney,[1] G. Lüpke,[1,2] N. H. Tolk,[1] and L. C. Feldman[1,3]
[1] *Department of Physics and Astronomy, Vanderbilt University, Nashville, Tennessee 37235*
[2] *Department of Applied Science, The College of William and Mary, Williamsburg, Virginia 23187*
[3] *Solid State Division, Oak Ridge National Laboratory, Oak Ridge, Tennessee 37831*
(Received 31 October 2000; published 11 April 2001)

The absorption line shape associated with the fundamental transition of the H-related stretch mode of bond-center hydrogen in crystalline silicon is measured as a function of temperature with infrared spectroscopy. In addition to the shift in frequency and increase in linewidth usually observed for local vibrational modes in solids, the absorption line becomes asymmetric at elevated temperatures. A theoretical model is developed, which describes the temperature-dependent line shape in terms of thermal fluctuations in the occupation number of a low-frequency mode coupled anharmonically to the stretch mode. The model successfully describes the shift, broadening, and asymmetry of the absorption line and gives new insight into the nature of the low-frequency mode. The mode has a frequency of 114 cm^{-1}, is twofold degenerate, and exhibits no isotopic shift when deuterium is substituted for hydrogen. It is assigned to a pseudolocalized, Si-related mode of bond-center hydrogen.

DOI: 10.1103/PhysRevB.63.195203 PACS number(s): 61.72.Tt, 63.20.Pw, 78.30.Am

I. INTRODUCTION

Infrared spectroscopy of local vibrational modes (LVM's) is one of the most powerful techniques for studying the atomic-scale structure of light impurities and their complexes in crystalline solids.[1,2] One of the most prominent applications of LVM spectroscopy has been the investigation of H-related defects in crystalline semiconductors.[3–5] In this case, the combined information obtained from LVM spectroscopy and first-principles theoretical calculations[6] has led to the identification of a large number of H-related defects, including complexes of H with dopants,[7] transitions metals,[8] intrinsic defects,[9] and other H atoms.[10–12] Most of the investigations reported to date have focused on determining the defect structure, i.e., the equilibrium positions of the impurity atom(s) and the host atoms to which they are bonded. Such studies are usually based on measurements—at one particular cryogenic temperature—of the frequencies of the absorption lines, their isotopic shifts, and the splitting patterns induced by uniaxial stresses applied along low-index crystal axes.

Another characteristic feature of the infrared absorption spectrum, which has received much less attention, is its temperature dependence. Absorption lines associated with LVM's generally shift in frequency and broaden with increasing temperature. Moreover, the absorption lines may become asymmetric and, in rare cases, new absorption peaks appear next to the low-T line at elevated temperatures.[13,14] The T dependence of the line shape is generally attributed to random, thermal excitation and deexcitation of low-frequency vibrational modes that are coupled anharmonically to the LVM. Another possible cause of line broadening is the decrease in the lifetime of the first-excited state of the LVM, which sets in at elevated temperature.[15] Until recently the lifetimes of Si–H stretch modes were believed to be in the nanosecond range based on direct measurements of the lifetime of Si–H bonds on H-terminated Si surfaces.[16] Such lifetimes correspond to natural linewidths of the order 0.005 cm^{-1}, much less than the widths usually observed for LVM's in semiconductors, and the lifetime contribution to the T dependence of the linewidth has therefore been neglected until now. However, as we have recently shown, the vibrational lifetimes of Si–H stretch modes associated with point defects in semiconductors can be 2–3 orders of magnitude shorter than on H-terminated Si surfaces, and the lifetime contribution to the widths of LVM's may be significant.[17]

In this work, we extend our recent investigations of the population dynamics of the H-related stretch mode of bond-center hydrogen ($H_{BC}^{(+)}$) in Si at 1998 cm^{-1}, reported in Ref. 17, to also include phase relaxation dynamics. $H_{BC}^{(+)}$ in Si has been studied extensively experimentally[17–24] and theoretically,[6,25–29] and is very well characterized. The properties of $H_{BC}^{(+)}$ were recently reviewed in Ref. 22 and shall therefore not be repeated here. In this work, the absorption line shape of the 1998-cm^{-1} mode of $H_{BC}^{(+)}$ is measured with infrared absorption spectroscopy as a function of temperature. The T-dependent lifetime contribution to the linewidth obtained in Ref. 17 is subtracted from the measured linewidth, and the T dependence of the corrected width and the center frequency is analyzed in terms of the exchange model for vibrational phase relaxation developed by Harris and co-workers,[30–32] which assumes that the phase relaxation is governed by thermal fluctuations in the population number of one particular low-frequency mode coupled anharmonically to the LVM. However, the Harris theory is a low-T approximation and turns out to be invalid in almost the entire temperature range studied in the present work. We therefore extend the theory beyond the low-T limit. In addition to modifying the theoretical expressions for the line shift and broadening, the extended theory gives an explicit formula for the line shape function that allows the line shape to be asymmetric. The absorption line shape of the 1998-cm^{-1} mode of $H_{BC}^{(+)}$ agrees very well with this theoretical line shape function at all temperatures. The parameter determining the

asymmetry of the line is found to be a factor of 2 less than observed experimentally. This discrepancy originates from the degeneracy of the low-frequency mode: in the exchange theory of Harris and co-workers, and all other dephasing theories reported to date, the low-frequency mode has implicitly been assumed to be nondegenerate. However, the present work demonstrates that the predictions of the exchange model depend critically on the degeneracy of the low-frequency mode, and the discrepancy in the asymmetry parameter is removed if the low-frequency mode is assumed to be twofold degenerate instead of nondegenerate. The T dependence predicted by the extended exchange model is in excellent agreement with the behavior of the 1998-cm^{-1} line of $H_{BC}^{(+)}$ up to $\sim$100 K. From this we conclude that the phase relaxation of the 1998-cm^{-1} mode is governed by anharmonic coupling to a twofold degenerate mode at 114 cm^{-1}. The frequency of the low-frequency mode does not change when D is substituted for H, and we therefore assign it to a vibrational mode of the Si atoms in the immediate vicinity of the defect.

II. HOMOGENEOUS LINE SHAPE OF DIPOLE TRANSITIONS

In this section, the theory of homogeneous spectral line shapes of electric dipole transitions is reviewed. The theory has been applied to a wide variety of transitions, including transitions between nuclear and electronic spin states, vibrational states in gases and solids, and electronic states. In the present context we focus on the fundamental transition $|0\rangle \rightarrow |1\rangle$ of a LVM in a solid. The absorption spectrum associated with the fundamental excitation of a LVM can generally be expressed as the Fourier transform of the dipole-dipole correlation function:[33,34]

$$I_{|0\rangle\rightarrow|1\rangle}(\omega) \propto \int_{-\infty}^{\infty} dt \exp(i\omega t)\langle \mu_{01}(0)\mu_{01}^{*}(t)\rangle, \qquad (1)$$

where ω is the angular frequency, and $\mu_{01}(0) = \langle 0|\hat{\mu}(0)|1\rangle$ and $\mu_{01}^{*}(t) = \langle 0|\hat{\mu}^{\dagger}(t)|1\rangle$ are the expectation values of the dipole operator $\hat{\mu}$ and its Hermitian conjugate at time 0 and t. The bracket $\langle \cdots \rangle$ means that the function $\mu_{01}(0)\mu_{01}^{*}(t)$ has to be averaged over all possible time evolutions, which corresponds to performing an ensemble average. The dipole-dipole correlation function can be expressed as

$$\langle \mu_{01}(0)\mu_{01}^{*}(t)\rangle = \exp(i\omega_{01}t)\varphi_{01}(t). \qquad (2)$$

Here, the exponential term is the time dependence of the unperturbed LVM, whereas the function $\varphi_{01}(t)$ represents the effect of anharmonic interactions with other normal modes, which cause the amplitude of $\langle \mu_{01}(0)\mu_{01}^{*}(t)\rangle$ to decay. The decay of the correlation function can be viewed as a loss of phase coherence among the oscillators of the ensemble, and is often referred to as dephasing. In this paper we are only concerned with the homogeneous line shape and neglect inhomogeneous broadening of the absorption line, e.g., due to strain fields induced by nearby defects.

Phase relaxation processes are usually divided into two classes. The first class consists of those processes that change the quantum number of the LVM, thus causing the states of the mode to have finite lifetimes. For the fundamental transition of a normal mode, the decay function due to population relaxation processes is

$$\varphi_{01}^{T_1}(t) = z \exp\left[-\frac{t}{2T_1}\right], \qquad (3)$$

where T_1 is the lifetime of the first-excited state, and z is real. The second class of phase relaxation processes are caused by interactions that conserve the quantum number of the LVM. This type of phase relaxation is caused by anharmonic terms, which couple the LVM to other normal modes, thus causing the LVM transition frequency $\omega_{LVM} = -\omega_{01}$ to depend on the occupation numbers of the modes to which the LVM is coupled. Thermal fluctuations in the occupation numbers then give rise to fluctuations in the transition frequencies, which lead to loss of phase coherence and cause $\langle \mu_{01}(0)\mu_{01}^{*}(t)\rangle$ to decay. This type of phase relaxation is usually called ''pure dephasing,'' but for brevity we shall also use the abbreviated term ''dephasing'' in this paper. In Sec. V we show that the correlation function of such a randomly modulated transition can be expressed as

$$\varphi_{01}^{T_2^*}(t) = (z_{\mathrm{Re}} + iz_{\mathrm{Im}})\exp\left[i\Delta\omega_{01}t - \frac{t}{T_2^*}\right], \qquad (4)$$

where z_{Re}, z_{Im}, $\Delta\omega_{01}$, and T_2^* are real. T_2^* is the relaxation time due to (pure) dephasing. Population relaxation and dephasing are usually treated as independent processes, and the combined dipole-dipole correlation function can therefore be written as

$$\langle \mu_{01}(0)\mu_{01}^{*}(t)\rangle = \exp[i\omega_{01}t]\varphi_{01}^{T_1}(t)\varphi_{01}^{T_2^*}(t). \qquad (5)$$

Insertion of Eqs. (3)–(5) into Eq. (1) yields the homogeneous line shape function[35]

$$I_{|0\rangle\rightarrow|1\rangle}(\omega) \propto z_{\mathrm{Re}}\left[\frac{\Gamma/2}{(\omega-[\omega_{LVM}-\Delta\omega_{01}])^2+(\Gamma/2)^2} - a\frac{(\omega-[\omega_{LVM}-\Delta\omega_{01}])}{(\omega-[\omega_{LVM}-\Delta\omega_{01}])^2+(\Gamma/2)^2}\right], \qquad (6)$$

where

$$\Gamma = \frac{2}{T_2^*} + \frac{1}{T_1}. \qquad (7)$$

Thus, the homogeneous line shape is a Lorentzian centered at $\omega_{LVM}-\Delta\omega_{01}$ with full width at half maximum (FWHM) Γ, plus an asymmetric dispersion-type line shape defined by the same parameters. Hence, dephasing can cause the absorption line to broaden, shift in frequency, and become asymmetric. The amplitude of the asymmetric part is given by the parameter $a \equiv z_{\mathrm{Im}}/z_{\mathrm{Re}}$, and the homogeneous line shape therefore reduces to a Lorentzian if $z_{\mathrm{Im}} \rightarrow 0$.

TABLE I. Sample implantation conditions. Going from left to right, the columns contain the name of the sample, implanted ion, minimum implantation energy, maximum implantation energy, number of energies, width of implantation profile, hydrogen concentration, implantation temperature, and the location where the experiment was performed.

Sample name	Ion	E_{min} (MeV)	E_{max} (MeV)	Number of energies	Width (μm)	C_H (ppm)	T_{impl} (K)	Location
SiH 1	H^+	1.0	1.8	29	24	8.3	80	Vanderbilt
SiH 2	H^+	1.2	2.8	57	44	14	20	Aarhus
SiD[a]	D^+	6.0	10.8	46	316	1.3	20	Aarhus

[a]Implanted through a 100-μm-thick Al foil

Although vibrational frequencies and photon energies conventionally are expressed in wave number units (cm^{-1}) in infrared spectroscopy, we shall almost exclusively use angular frequencies (rad/s) in the theoretical expressions given in the present paper. Angular frequencies are readily converted to wave number units by division with $2\pi c$, where c is the speed of light in free space. Thus, the homogeneous linewidth (7) takes the form

$$\Gamma_\sigma = \frac{\Gamma}{2\pi c} = \frac{1}{\pi c T_2^*} + \frac{1}{2\pi c T_1}. \tag{8}$$

Expressions (7) and (8) for the Lorentzian part of the line shape function have been used extensively in the past, e.g., in studies of absorption lines associated with vibrational modes of adsorbates on surfaces[36] and molecular crystals.[37] However, to our knowledge, the homogeneous line shape function (6) has not been specified previously. In Sec. IV we use Eq. (6) in the analysis of the temperature-dependent shape of the 1998-cm^{-1} line of $H_{BC}^{(+)}$ in Si. We find that the 1998-cm^{-1} line becomes significantly asymmetric at elevated temperatures and that Eq. (6) represents the observed line shape very well at all temperatures. The best-fit line shape parameters a, $\Delta\omega_{01}$, and Γ are strongly dependent on the temperature at which the absorption spectrum is measured. To understand the physical processes giving rise to this T dependence, we develop a theoretical model in Sec. V, which expresses the temperature dependence of the line shape parameters in terms of well-defined physical quantities.

III. EXPERIMENTAL DETAILS

$H_{BC}^{(+)}$ in Si is unstable at room temperature and therefore has to be formed and kept at cryogenic temperatures to prevent it from migrating and reacting with impurities and defects. This is accomplished by implanting protons (or deuterons) into Si at 80 K or below, where they freeze in at bond-center sites forming $H_{BC}^{(+)}$ (or $D_{BC}^{(+)}$). The absorption spectra are measured *in situ*, i.e., without heating the sample to room temperature between implantation and the spectroscopic measurements. The samples used in the present work consisted of 2-mm-thick, double-side polished, high-resistivity ($>600\ \Omega$ cm) Si single crystals. To facilitate the transfer of the implanted sample to the infrared spectrometer without heating, the sample was mounted in a cryostat that could be attached to the end of the accelerator beam line. A gate valve was mounted between the cryostat and the beam line, which allowed the ions to pass while the valve was open and made possible detachment of the cryostat from the beam line, without breaking the cryostat vacuum, with the valve closed. For practical reasons the gate valve was replaced by a 100-μm-thick Al foil, in the case of the deuteron-implanted sample, with the deuterons penetrating the foil before being implanted into the Si sample. The ion beam was swept horizontally and vertically during implantation to ensure a uniform lateral distribution of the implanted species. To minimize the defect concentration, while maintaining a sufficient area density of $H_{BC}^{(+)}$ or $D_{BC}^{(+)}$ defects for the spectroscopic studies, the spatial profile of implanted ions was spread out longitudinally by implanting at multiple energies. The dose at each energy was obtained from Monte Carlo simulations of the implantation profiles with the software package SRIM,[38,39] and were chosen to yield a uniform hydrogen or deuterium concentration profile over the depth interval defined by the ion range at the minimum and maximum implantation energy. The implantation parameters for the samples are given in Table I.

The experiments at Vanderbilt University were performed with a flow cryostat cooled with liquid He, whereas a closed-cycle cryostat was used for the experiments at Aarhus University. Both cryostats were capable of cooling the sample to $\sim$10 K. The sample temperature was measured with Si diodes mounted on the sample holder a few millimeters from the sample. The cryostats were equipped with a resistive heater, controlled by a commercial temperature controller, which allowed the temperature to be set at any temperature in the range 10–300 K. The measured temperature was generally stable within ± 0.05 K. The cryostats were equipped with a pair of windows (CsI or CaF_2) mounted perpendicularly to the implantation port. After implantation, the cryostat was detached from the beam line, and the cold finger and sample holder of the cryostat was rotated by 90° to allow the infrared light to propagate through the windows and the implanted sample. Then, the cryostat was moved to the commercial Fourier transform infrared (FTIR) spectrometer used for the absorption measurements. The sample temperature increased by less than 10 K during the transfer of the cryostat. The infrared absorbance spectra of the samples were measured as a function of sample temperature in the range 10–135 K. The spectral resolution was chosen to yield negligible instrumental broadening of the absorption lines, and

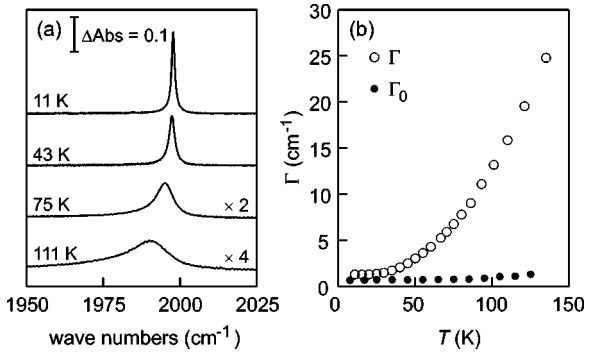

FIG. 1. (a) Absorbance spectra showing the 1998-cm^{-1} line of $H_{BC}^{(+)}$ at various temperatures. (b) Linewidth parameter Γ as a function of temperature (○) and lifetime contribution to the linewidth (●) obtained from Eq. (9) and the T_1 values reported in Ref. 17.

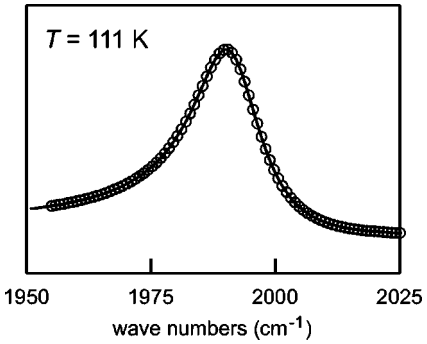

FIG. 2. Absorbance spectrum at $T=111$ K showing the asymmetry of the 1998-cm^{-1} line. The circles represent the measured spectrum, whereas the curve is the best fit of the line shape function (6) to the data.

ranged from 0.3 at the lowest to 1.0 cm^{-1} at the highest temperatures.

IV. EXPERIMENTAL DATA

The homogeneous shape of an absorption line is determined by a combination of population and pure dephasing processes. In the case of vibrational transitions in solids, pure dephasing processes vanish in the low-T limit ($\lim_{T\to 0} T_2^* = \infty$), because all vibrational degrees of freedom freeze into the ground state.[37] Hence, it follows from Eqs. (6) and (7) that the low-T homogeneous line shape is Lorentzian with a FWHM given by the natural linewidth

$$\Gamma_0 = \frac{1}{T_1}. \tag{9}$$

In a recent Letter we confirmed this relation experimentally for the 1998-cm^{-1} line of $H_{BC}^{(+)}$ in Si by directly measuring T_1 and the spectral width at low temperatures.[17] The lifetime was measured to be $T_1 = 7.8 \pm 0.2$ ps at ~ 20 K by ultrafast, time-resolved infrared spectroscopy. Infrared absorption measurements at ~ 10 K revealed that the shape of the 1998-cm^{-1} line was very well represented by a Lorentzian, and that the width of the line converged towards Γ_0 when the implanted hydrogen concentration was reduced to ~ 1 ppm. The temperature dependence of T_1 was also measured, and T_1 was found to be essentially temperature independent up to ~ 60 K, where it started to decrease. At 125 K the lifetime was reduced to ≈ 4 ps.

Figure 1(a) shows the absorbance profile of the 1998-cm^{-1} line measured at various temperatures. The line shape is strongly temperature dependent, exhibiting a large downshift in frequency of 6 cm^{-1} and increase in width of 15 cm^{-1}, when the temperature is raised from 10 to 111 K. Moreover, the line shape changes from being an almost perfect Lorentzian at low temperatures to being significantly asymmetric at elevated temperatures. As an example of the asymmetric line shape, Fig. 2 shows the 1998-cm^{-1} line measured at 111 K. The curve in the figure represents the best fit of Eq. (6) to the experimental data. The fits obtained at all the other temperatures were of similar or better quality. Thus, the experimental line shapes are very well represented by the homogeneous line shape function (6) at all temperatures. Figure 1(b) shows the measured linewidth Γ and the natural linewidth Γ_0 as a function of temperature. Γ_0 was calculated from Eq. (9) and the T_1 data reported in Ref. 17. The temperature dependence of T_1 is clearly much too weak to explain the broadening of the 1998-cm^{-1} line with increasing temperature. Consequently, the line shape is primarily determined by pure dephasing processes above ~ 50 K. The change in linewidth due to pure dephasing $\Delta\Gamma^{T_2^*}$ can be extracted from the widths Γ by subtraction of the natural linewidth Γ_0 and the contribution from inhomogeneous broadening. The temperature dependence of the natural linewidth is represented by the function

$$\Gamma_0[T] = \Gamma_0^{LT} \frac{\exp[\hbar\omega_{LVM}/k_B T] - 1}{\prod_{j=1}^{6} (\exp[\hbar\omega_j/k_B T] - 1)}, \tag{10}$$

where k_B is the Boltzmann constant, $\omega_{LVM} = 1998$ cm^{-1}, $\omega_1 = \omega_2 = \omega_3 = 150$ cm^{-1}, $\omega_4 = \omega_5 = \omega_6 = 516$ cm^{-1}, and Γ_0^{LT} is obtained from Eq. (9) and the experimental low-T lifetime $T_1 = 7.8 \pm 0.2$ ps. As demonstrated in Ref. 17, Eq. (10) represents the temperature dependence of T_1, and hence the natural linewidth, quite well. The inhomogeneous broadening corresponds to the difference between Γ and Γ_0 below 30 K, shown in Fig. 1(b), and is assumed to be independent of temperature.

As already mentioned, pure dephasing processes can cause a T-dependent shift of absorption line frequencies. In addition, vibrational frequencies of LVM's are expected to change with temperature because of thermal expansion of the host lattice, which changes the lengths of the bonds between the impurity and the host atoms, and thus the LVM frequencies. The latter contribution to the line shift can be calculated if the thermal expansion coefficient and elastic constants of the host crystal, and the sensitivity of the 1998-cm^{-1} line to strain are known. In Appendix A it is shown that the shift due to thermal expansion is at least two orders of magnitude

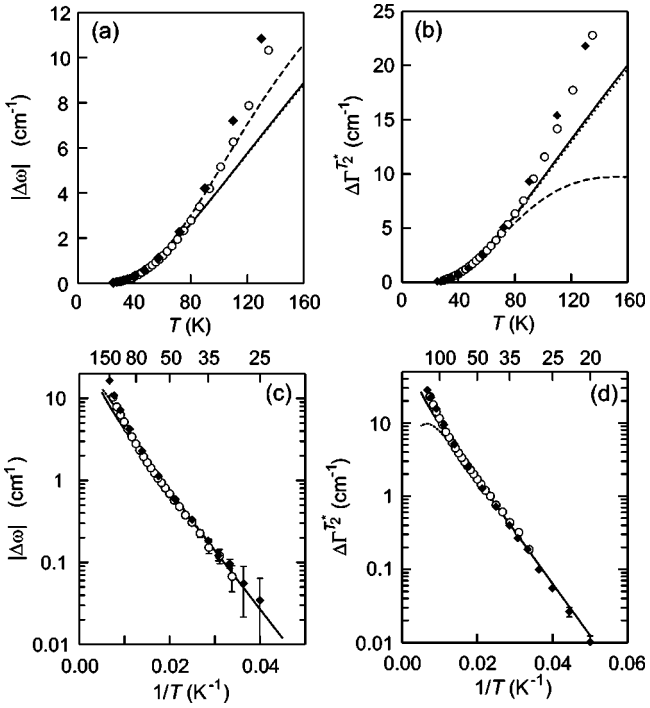

FIG. 3. Temperature dependence of the line shape parameters of the 1998-cm^{-1} line. (a) Frequency shift $|\Delta\omega|=|\omega-\langle\omega\rangle_{LT}|$ vs T, where $\langle\omega\rangle_{LT}$ is the low-T mean frequency obtained by averaging over four measurements of ω in the range 10–30 K. (b) Change in linewidth due to dephasing, $\Delta\Gamma^{T_2^*}=\Gamma-\Gamma_0-\Gamma^{inhom}$, as a function of T. Here, Γ_0 is the T-dependent natural linewidth given by Eq. (10), and $\Delta\Gamma^{inhom}$ represents the contribution to the width from inhomogeneous broadening. (c) and (d) show semilogarithmic plots of the same data as (a) and (b) as a function of 1/T. The two data sets were obtained with the two proton-implanted samples SiH 1 (♦) and SiH 2 (○) listed in Table I. The solid curves represent the best-fit theoretical results obtained with the exchange model and a nondegenerate exchange mode. The number of exchange mode levels ($n_e^{max}+1$) was chosen large enough that the model results were independent of n_e^{max}. The dotted curves, which essentially coincide with the solid curves, show the model predictions for a twofold degenerate exchange mode. The best-fit parameters are listed in Table II. The dashed curves show the results obtained with the two-level exchange model, i.e., with $n_e^{max}=1$.

smaller than the shifts observed. We therefore neglect this contribution and ascribe the experimental shifts to pure dephasing.

Figures 3(a,b) show the absolute value of the frequency shift $|\Delta\omega|$ and the pure dephasing contribution to the linewidth $\Delta\Gamma^{T_2^*}$ as a function of temperature. The behavior at low temperature is presented more clearly by semilogarithmic plots of the data as a function of 1/T [see Figs. 3(c,d)]. Two data sets are shown in the figures, which were obtained with the two different cryostats. The data are in excellent agreement below ~100 K, indicating that systematic errors in the temperature measurements are very small. The deviations between the data sets above ~100 K, are probably due to differences in cryostat and sample holder design. However, only the data below ~80 K are used in the quantitative analysis, and the errors at elevated temperatures therefore have no influence on the conclusions of the present paper.

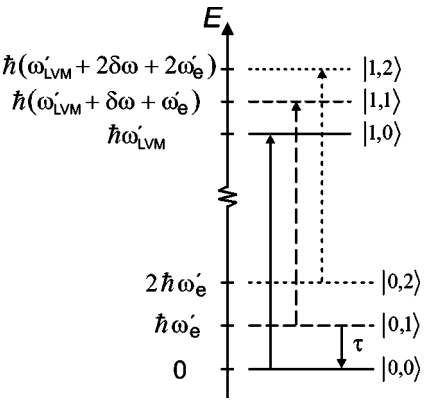

FIG. 4. Energy-level diagram of the exchange model defining the three model parameters ω'_e, $\delta\omega$, and τ. The level spacing in the LVM ground-state manifold $|0,n_e\rangle$ is $\hbar\omega'_e$, whereas it is $\hbar\omega'_e+\delta\omega$ in the LVM singly-excited manifold $|1,n_e\rangle$. Thus, the transition energy for the electric dipole transition $|0,n_e\rangle\rightarrow|1,n_e\rangle$ is equal to $\hbar(\omega'_{LVM}+n_e\delta\omega)$. The parameter τ is the spontaneous lifetime of the $|0,1\rangle$ level. For simplicity, only three levels in each manifold are shown. In the model of Harris *et al.*, only two exchange-mode levels $|n_{LVM},0\rangle$ and $|n_{LVM},1\rangle$ are taken into account ($n_e^{max}=1$), whereas the extended exchange model includes as many levels as required to make the model predictions independent of n_e^{max}.

According to Fig. 3(c,d), the data points representing the frequency shift and line broadening in the temperature range 30–80 K fall on a straight line in the semilogarithmic plots of $|\Delta\omega|$ and $\Delta\Gamma^{T_2^*}$ versus 1/T. Thus, both quantities exhibit Arrhenius-type behavior and can be expressed as $A^{(j)}\exp[-\hbar\Omega^{(j)}/k_BT]$ in this regime. A quantitative analysis[39] yields the best-fit parameters $\Omega^{(|\Delta\omega|)}=114\pm2$ cm^{-1} and $\Omega^{(\Delta\Gamma)}=117\pm2$ cm^{-1}, which shows that $\Omega^{(|\Delta\omega|)}$ and $\Omega^{(\Delta\Gamma)}$ are equal within the experimental errors. This behavior is in excellent agreement with the theoretical models of vibrational dephasing developed by Harris and co-workers[30–32] and by Persson and co-workers.[41]

Both models assume that the LVM is coupled anharmonically to another vibrational mode with frequency ω_e, where $\omega_e\ll\omega_{LVM}$. The anharmonic coupling changes the energy level spacings as shown in Fig. 4. In the manifold $|0,n_e\rangle$, $n_e\in\{0,1,\ldots\}$, in which the LVM is in the ground state, the anharmonic coupling term changes the level spacing from $\hbar\omega_e$ to $\hbar\omega'_e\equiv\hbar(\omega_e+\frac{1}{2}\delta\omega)$, whereas the spacing in the $|1,n_e\rangle$ manifold is $\hbar(\omega'_e+\delta\omega)$. As explained in more detailed later, $\delta\omega$ is determined by the strength and type of the anharmonic coupling. According to Fig. 4, the transition energy for fundamental transitions of the LVM, $|0,n_e\rangle\rightarrow|1,n_e\rangle$, are given by $\Delta E_{|0,n_e\rangle\rightarrow|1,n_e\rangle}=\hbar(\omega'_{LVM}+n_e\delta\omega)$, where $\omega'_{LVM}\equiv\omega_{LVM}+\frac{1}{2}\delta\omega$. Thus, the fundamental transition energy of the LVM depends on the quantum number n_e of the low-frequency mode, and thermal fluctuations in n_e lead to a random modulation of the transition energy, which in turn results in loss of phase coherence. In addition to ω_e and $\delta\omega$, the lifetime τ of the $n_e=1$ state of low-frequency mode enters as a model parameter.

A. The model of Harris and co-workers

Harris and co-workers showed that in the limit $k_BT \ll \hbar\omega_e'$, the pure dephasing contribution to the homogeneous line shape is Lorentzian, and exhibits a temperature-dependent frequency shift and broadening given by[30–32]

$$\Delta\omega = \frac{\delta\omega}{1+(\delta\omega\tau)^2}\exp[-\hbar\omega_e'/k_BT] \tag{11}$$

and

$$\Delta\Gamma^{T_2^*} = \frac{2\delta\omega^2\tau}{1+(\delta\omega\tau)^2}\exp[-\hbar\omega_e'/k_BT]. \tag{12}$$

As mentioned above, a fit of Eqs. (11) and (12) to the experimental data yields $\omega_e' \sim 115\ \mathrm{cm}^{-1}$. Thus, the assumption $k_BT \ll \hbar\omega_e'$, corresponding to $T \ll 160$ K, is not fulfilled for any of the data points shown in Fig. 3. However, the excellent agreement below 80 K suggests that the model of Harris and co-workers contains the essential physics governing the T dependence of the line shape. In the following sections we will extend this model beyond the low-T limit.

B. The model of Persson and co-workers

Persson and co-workers derived the frequency shift and broadening due to vibrational exchange in the weak coupling limit $|\delta\omega\ \tau| \ll 1$, and obtained the results

$$\Delta\omega = \delta\omega\bar{n}_e[T] \tag{13}$$

and

$$\Delta\Gamma^{T_2^*} = 2\delta\omega^2\tau\bar{n}_e[T](\bar{n}_e[T]+1), \tag{14}$$

where $\bar{n}_e[T] = (\exp[\hbar\omega_e'/k_BT]-1)^{-1}$ is the mean population number of the exchange mode in thermal equilibrium. Expressions (13) and (14) are valid at all temperatures. Both models of Harris and co-workers and of Persson and co-workers both yield $\Delta\Gamma^{T_2^*}/\Delta\omega = 2\delta\omega\ \tau$ in the low-T limit, and the coupling parameter $\delta\omega\,\tau$ can therefore be obtained from this ratio. Experimentally, we find $\delta\omega\,\tau = -1.2$ for the 1998-cm line. Consequently, the model of Persson and co-workers cannot be used to analyze the T dependence of the 1998-cm^{-1} line of $H_{BC}^{(+)}$ in Si.

V. DEPHASING BY RANDOM FREQUENCY MODULATION

In this section the dephasing model of Harris and co-workers is extended beyond the low-T limit. The main reason for the breakdown of this model is that the first-excited state of the low-frequency mode becomes significantly populated when $k_BT \sim \hbar\omega_e'$, which makes possible thermal excitation into states with $n_e \geqslant 2$. Hence, the crucial step in extending the model is to increase the quantum number n_e^{max} above which the low-frequency mode is truncated from $n_e^{max} = 1$, as assumed by Harris and co-workers, to a number sufficiently large for the results to be independent of n_e^{max}. In this case, no simple analytical expressions for the line shape parameters like Eqs. (11) and (12) can be given. However, the homogeneous line shape function (6) remains approximately correct, and the frequency shift, linewidth, and the amplitude of the asymmetric function can be calculated numerically for any given T. For simplicity, the following derivation is first carried out assuming a nondegenerate exchange mode. Subsequently, the theory is generalized to the case of a twofold degenerate exchange mode.

A. The exchange model

The Hamiltonian of the model system, for which the homogeneous line shape is derived, is assumed to be

$$\hat{H} = \hat{H}_0 + \hat{H}_{anh} + \hat{H}_{exch}. \tag{15}$$

Here, $\hat{H}_0$ is the zero-order, harmonic Hamiltonian consisting of the sum of all the normal-mode Hamiltonians of the silicon crystal with a $H_{BC}^{(+)}$ defect:

$$\hat{H}_0 = \sum_i \tfrac{1}{2}\frac{\partial^2}{\partial Q_i^2} + \tfrac{1}{2}\omega_i^2 Q_i^2,$$

where Q_i is the normal-mode coordinate of the mode i, and ω_i is its frequency. $\hat{H}_{anh}$ consists of anharmonic terms which couple the LVM with a single low-frequency mode with frequency ω_e, also called *the exchange mode* for reasons that will become apparent later. $\hat{H}_{anh}$ can generally be expressed in terms of normal coordinates as

$$\hat{H}_{anh} = \sum_{l,m} C_{l,m} Q_{LVM}^l Q_e^m, \tag{16}$$

where the sum extends over combinations of l and m with $l+m>2$, but we shall limit the present discussion to terms of the type $C_{2,2}Q_{LVM}^2 Q_e^2$ and $C_{2,1}Q_{LVM}^2 Q_e$. Symmetry does not impose any restrictions on the existence of terms of the first type, whereas the second type only exists if the exchange mode has A_{1g} symmetry.[31]

The final term, $\hat{H}_{exch}$, of the system Hamiltonian couples the exchange mode to the ''phonon bath'' consisting of all the other normal modes of the system, and ensures that the exchange mode is in thermal equilibrium with the bath. We assume that the equilibration of the exchange mode takes place through *exchange* of single vibrational quanta with the phonon modes characterized by a vector $\vec{\mathbf{k}}$ and a branch index s, i.e., $n_e \to n_e \pm 1$ and $n_{\vec{\mathbf{k}},s} \to n_{\vec{\mathbf{k}},s} \mp 1$, where n_e and $n_{\vec{\mathbf{k}},s}$ are the quantum numbers of the exchange mode and the phonon modes. The simplest type of $\hat{H}_{exch}$ that has this property is

$$\hat{H}_{exch} = \sum_{\vec{\mathbf{k}},s} \alpha_{\vec{\mathbf{k}},s} Q_e Q_{\vec{\mathbf{k}},s} = \sum_{\vec{\mathbf{k}},s} \alpha_{\vec{\mathbf{k}},s} \sqrt{\frac{\hbar^2}{4\omega_e\omega_{\vec{\mathbf{k}},s}}}(\hat{a}_e^\dagger + \hat{a}_e)(\hat{a}_{\vec{\mathbf{k}},s}^\dagger + \hat{a}_{\vec{\mathbf{k}},s}), \tag{17}$$

where the creation and annihilation operators $\hat{a}_j^\dagger$ and $\hat{a}_j$ of the modes have been introduced, and $\alpha_{\vec{\mathbf{k}},s}$ are constants related to the lifetime τ of the exchange mode.

B. Time dependence of the dipole moment

Having defined the system of interest, we will now use the Hamiltonian (15) to derive an expression for the homogeneous line shape $I_{|0\rangle\rightarrow|1\rangle}$ of the fundamental transition of the LVM. We first calculate $\mu_{01}(t)$, i.e., the expectation value of the dipole operator $\hat{\mu}$ at time t. The time evolution of the matrix $\boldsymbol{\mu}$ representing the dipole operator is given by

$$i\hbar\frac{d\boldsymbol{\mu}}{dt}=[\mathbf{H},\boldsymbol{\mu}],$$

where $\mathbf{H}$ is the matrix representation of $\hat{H}$. Following Anderson,[33] the solution to this differential equation can be written as[42]

$$\mu_{ij}(t)=(\boldsymbol{\mu}(t))_{i,j}=\mu_{ij}(0)\exp\left[-i\left(\omega_{ij}t+\int_0^t\Delta\omega_{ij}(t')dt'\right)\right], \tag{18}$$

where

$$\omega_{ij}\equiv[(\mathbf{H}_0)_{i,i}-(\mathbf{H}_0)_{j,j}]/\hbar$$

and

$$\Delta\omega_{ij}(t')\equiv[(\mathbf{H}_{anh}(t'))_{i,i}-(\mathbf{H}_{anh}(t'))_{j,j}]/\hbar,$$

which for the fundamental transition reduces to

$$\omega_{01}=-\omega_{LVM} \tag{19}$$

and

$$\Delta\omega_{01}(t')=-\delta\omega[n_e(t')+\tfrac{1}{2}]. \tag{20}$$

Here, it has been used that $\mathbf{H}_{anh}(t')$ depends on time through the time dependence of n_e. The variable $\delta\omega$ appearing on the right-hand side of Eq. (20) depends on the type of anharmonic coupling between the LVM and exchange mode. If $\hat{H}_{anh}=C_{2,2}Q_{LVM}^2Q_e^2$, then $\delta\omega$ can be calculated using first-order perturbation theory and is given by

$$\delta\omega=\frac{C_{2,2}\hbar}{\omega_{LVM}\omega_e}. \tag{21}$$

If, instead, $\hat{H}_{anh}=C_{2,1}Q_{LVM}^2Q_e$, then the first-order contribution vanishes, and $\delta\omega$ has to be calculated by second-order perturbation theory, which gives

$$\delta\omega=\frac{-2C_{2,1}^2\hbar}{4\omega_{LVM}^3\omega_e-\omega_{LVM}\omega_e^3}. \tag{22}$$

Notice, that Eq. (22) implies that $\delta\omega$ is negative, whereas $\delta\omega$ can be either positive or negative if $\hat{H}_{anh}=C_{2,2}Q_{LVM}^2Q_e^2$, depending on the sign of $C_{2,2}$.

Combining Eqs. (18)–(20), the time dependence of the dipole moment can be written as

$$\mu_{01}(t)=\mu_{01}(0)\exp\left[i\omega'_{LVM}t+i\delta\omega\int_0^t n_e(t')dt'\right].$$

According to this equation, $\mu_{01}(t)$ consists of two t-dependent factors; an oscillatory term with frequency ω'_{LVM} that determines the center frequency of the absorption line in the limit $T\rightarrow 0$, and a term that depends on the fraction of the time that the exchange mode is in one of its excited states. Thus, the temperature dependence of the line shape is caused by the change in occupation number of the exchange mode.

C. Dipole-dipole correlation function

The next step in the derivation of the homogeneous line shape is to calculate the ensemble average of $\mu_{01}(0)\mu_{01}^*(t)$. To this end, we again follow the approach devised by Anderson in Ref. 33. In short, the time interval t is divided into k subintervals of equal length t/k, where t/k is much shorter than the time scale of population transfer between the levels of the exchange mode. If the transition rates between the various levels are known, one can calculate the probability for a given sequence of population numbers $\{n_e[1],n_e[2],\ldots,n_e[k]\}$ to occur, where $n_e[m]$ is the occupation number in the mth interval. For such a sequence,

$$\mu_{01}(0)\mu_{01}^*(t)=|\mu(0)|^2\exp[-i\omega'_{LVM}t]\times\exp\left[-i\frac{\delta\omega t}{k}\sum_{m=1}^{k}n_e[m]\right].$$

The ensemble average is calculated by performing a weighted average over all possible sequences, with the weight of each contribution given by the probability $\mathcal{P}(n_e[1],\ldots,n_e[k])$ for that particular sequence to occur. Assuming that n_e is a Markovian random function,[43] this probability is

$$\mathcal{P}(n_e[1],\ldots,n_e[k])=p(n_e[1])P_{n_e[2],n_e[1]}\times P_{n_e[3],n_e[2]}\ldots P_{n_e[k],n_e[k-1]},$$

where $p(n_e[1])$ is the thermal-equilibrium probability for the exchange mode to be in state $n_e[1]$:

$$p(n_e[1])=(1-\exp[-\hbar\omega'_e/k_BT])\exp(-\hbar\omega'_en_e[1]/k_BT), \tag{23}$$

and $P_{n_e[m],n_e[m-1]}$ is defined as the probability that the occupation number of the exchange mode is $n_e[m]$ in the mth interval provided that it attained the value $n_e[m-1]$ in the preceding time interval, which is given by[33]

$$P_{n_e[m],n_e[m-1]}=\delta_{n_e[m],n_e[m-1]}+W_{n_e[m],n_e[m-1]}\frac{t}{k}.$$

Here, $W_{n_e[m],n_e[m-1]}$ is the transition probability for the transition $n_e[m-1]\rightarrow n_e[m]$. Using Fermi's golden rule, the operator (17), and the principle of detailed balance, it can be shown[44] that

$$W_{n_e[m],n_e[m-1]} = -\frac{1}{\tau}(n_e[m]+\overline{n_e}+2n_e[m]\overline{n_e})\,\delta_{n_e[m],n_e[m-1]} + \frac{1}{\tau}(n_e[m]+1)(\overline{n_e}+1)\,\delta_{n_e[m],n_e[m-1]-1} + \frac{1}{\tau}n_e[m]\overline{n_e}\,\delta_{n_e[m],n_e[m-1]+1}, \tag{24}$$

where $\overline{n_e}=[\exp(\hbar\omega_e'/k_BT)-1]^{-1}$ is the mean occupation number of the exchange mode. From Eq. (24) it follows that $\lim_{T\to 0}W_{0,1}=1/\tau$, which identifies τ as the spontaneous lifetime of the $n_e=1$ state of the exchange mode.

The ensemble average of the dipole-dipole correlation function $\langle\mu_{01}(0)\mu_{01}^*(t)\rangle$ is now calculated as the weighted average of the correlation functions $\mu_{01}(0)\mu_{01}^*(t)$ of the individual population sequences:

$$\langle\mu_{01}(0)\mu_{01}^*(t)\rangle = \sum_{n_e[1]=0}^{\infty}\ \cdots\ \sum_{n_e[m]=0}^{\infty} \times\mathcal{P}(n_e[1],\ldots,n_e[k])\,\mu_{01}(0)\mu_{01}^*(t),$$

which can be expressed as[33]

$$\langle\mu_{01}(0)\mu_{01}^*(t)\rangle = |\mu_{01}(0)|^2 \times\exp[-i\omega_{LVM}'t]\vec{\mathbf{p}}^T\exp[(\mathbf{W}^T-i\boldsymbol{\delta\omega})t]\vec{\mathbf{1}}. \tag{25}$$

Here, $\mathbf{W}^T$ is the transpose of the transition probability matrix defined in Eq. (24), $\boldsymbol{\delta\omega}$ is the diagonal matrix with elements $\boldsymbol{\delta\omega}_{l,m}=m\,\delta\omega\,\delta_{l,m}$, $\vec{\mathbf{p}}^T$ is the row vector $\{p(0),p(1),\ldots\}$ with components defined by Eq. (23), and $\vec{\mathbf{1}}$ is a column vector with all components equal to unity. Notice that $\langle\mu_{01}(0)\mu_{01}^*(t)\rangle$, apart from the constant $|\mu_{01}(0)|^2$, is uniquely determined by the three model parameters ω_e', $\delta\omega$, and τ, and the temperature T.

Twofold degenerate exchange mode

Until now it has been assumed implicitly that the exchange mode is nondegenerate. In reality this might not be the case. For instance, one of the likely exchange mode candidates, the bend mode of $H_{BC}^{(+)}$ where the H atom vibrates perpendicularly to the Si–H–Si bond axis, is twofold degenerate. In this subsection the exchange model is generalized to the case of a twofold degenerate exchange mode. As it turns out, the expression for the dipole-dipole correlation function (25) remains valid, but the vector $\vec{\mathbf{p}}$ and the matrices $\mathbf{W}$ and $\boldsymbol{\delta\omega}$ have to be redefined.

As in the case of a nondegenerate exchange mode, we assume that the twofold degenerate exchange mode is harmonic, except from the coupling to the stretch mode and the phonon bath given by Eqs. (16) and (17). We can therefore treat the exchange mode as two independent, nondegenerate vibrational modes with normal mode coordinates Q_{e1} and Q_{e2}, quantum numbers n_{e1} and n_{e2}, and with the same harmonic frequency ω_e. The cubic coupling term $C_{2,1}Q_{LVM}^2Q_e$ vanishes unless the exchange mode has A_{1g} symmetry. Consequently, we only have to consider quartic anharmonic coupling in the case of a degenerate exchange mode. We assume that the coupling interaction is given by

$$\hat{H}_{anh}=C_{2,2}Q_{LVM}^2(Q_{e1}^2+Q_{e2}^2),$$

which results in the level structure shown in Fig. 4, where $\delta\omega=\hbar C_{2,2}/(\omega_{LVM}\omega_e)$, $\omega_e'=\omega_e+\frac{1}{2}\delta\omega$, $\omega_{LVM}'=\omega_{LVM}+\delta\omega$, and the states $|n_{LVM},n_e\rangle$ indicated in the figure correspond to $|n_{LVM},n_{e1}+n_{e2}\rangle$. The equilibration of the degenerate exchange modes with the phonon bath is again assumed to take place through exchange of single vibrational quanta, and the exchange interaction is taken to be

$$\hat{H}_{exch}=\sum_{\vec{\mathbf{k}},s}\alpha_{\vec{\mathbf{k}},s}\sqrt{\frac{\hbar^2}{4\omega_e\omega_{\vec{\mathbf{k}},s}}}[(\hat{a}_{e1}^\dagger+\hat{a}_{e1})(\hat{a}_{\vec{\mathbf{k}},s}^\dagger+\hat{a}_{\vec{\mathbf{k}},s}) +(\hat{a}_{e2}^\dagger+\hat{a}_{e2})(\hat{a}_{\vec{\mathbf{k}},s}^\dagger+\hat{a}_{\vec{\mathbf{k}},s})].$$

The thermal-equilibrium probability of the exchange mode being in state $|n_{e1},n_{e2}\rangle$ is

$$p_E(n_{e1};n_{e2})=p(n_{e1})p(n_{e2}), \tag{26}$$

where $p(n_{ei})$ is given by Eq. (23). The transition probability for the $|n_{e1}',n_{e2}'\rangle\to|n_{e1},n_{e2}\rangle$ transition is

$$(W_E)_{(n_{e1};n_{e2}),(n_{e1}';n_{e2}')}=W_{n_{e1},n_{e1}'}\delta_{n_{e2},n_{e2}'}+W_{n_{e2},n_{e2}'}\delta_{n_{e1},n_{e1}'}, \tag{27}$$

where $W_{n_{ei},n_{ei}'}$ is defined in Eq. (24). The shift in transition frequency due to population of the exchange mode levels is

$$(\delta\omega_E)_{(n_{e1};n_{e2}),(n_{e1}';n_{e2}')}=\delta\omega(n_{e1}+n_{e2})\,\delta_{n_{e1},n_{e1}'}\delta_{n_{e2},n_{e2}'}. \tag{28}$$

The variables in Eqs. (26)–(28) can be expressed in matrix form by associating an index l with each pair of quantum numbers $(n_{e1};n_{e2})$. Thus, the matrix $\mathbf{W}_E$ can defined as $(\mathbf{W}_E)_{l,l'}\equiv(W_E)_{(n_{e1};n_{e2}),(n_{e1}';n_{e2}')}$. The matrix $\boldsymbol{\delta\omega}_E$ and the vector $\vec{\mathbf{p}}_E$ are defined in terms of Eqs. (26) and (28) in a similar way. The dipole-dipole correlation function of the exchange model with a twofold degenerate exchange mode is then simply given by Eq. (25) with $\mathbf{W}$, $\boldsymbol{\delta\omega}$, and $\vec{\mathbf{p}}$ replaced by $\mathbf{W}_E$, $\boldsymbol{\delta\omega}_E$, and $\vec{\mathbf{p}}_E$.

D. Absorption spectrum predicted by the exchange model

Having obtained the expression (25) for the dipole-dipole correlation function, the absorption spectrum can be calculated. In this section we show that the spectrum predicted by the exchange model can be approximated by the homogeneous line shape function (6), and show how the line shape parameters Γ, $\Delta\omega_{01}$, and a are related to the physical quantities ω_e', $\delta\omega$, τ, and T. Then, the exchange model is applied to analyze the T dependencies of the H-related stretch modes of $H_{BC}^{(+)}$ and $D_{BC}^{(+)}$ in Si. Finally, the approximate line shape is compared to the exact absorption spectrum of the exchange model.

1. Approximate line shape

The first step towards calculating the spectrum is to transform the matrix $\mathbf{M}=\mathbf{W}^T-i\boldsymbol{\delta\omega}$ to the basis defined by its eigenvectors. $\mathbf{M}$ can be expressed as $\mathbf{M}=\mathbf{T}\boldsymbol{\Lambda}\mathbf{T}^{-1}$, where $\boldsymbol{\Lambda}$ is the diagonal matrix with the eigenvalues λ_i of $\mathbf{M}$ as diagonal elements, and $\mathbf{T}$ is the transformation matrix with columns consisting of the eigenvectors of $\mathbf{M}$. Using this transformation,

$$\langle \mu_{01}(0)\mu_{01}^*(t)\rangle \propto \exp[-i\omega'_{LVM}t]\vec{\mathbf{p}}^T\mathbf{T}\exp[\boldsymbol{\Lambda}t]\mathbf{T}^{-1}\vec{\mathbf{1}}, \tag{29}$$

which can be written as

$$\langle \mu_{01}(0)\mu_{01}^*(t)\rangle \propto \sum_{l=1}^{l_{max}} z_l \exp[-i\omega'_{LVM}t+\lambda_l t], \tag{30}$$

where l_{max} is the dimension of the matrices $\mathbf{T}$, $\mathbf{M}$, $\mathbf{W}$, and $\boldsymbol{\delta\omega}$, which equals $n_e^{max}+1$ in the case of a nondegenerate exchange mode and $\frac{1}{2}(n_e^{max}+1)(n_e^{max}+2)$ if it is twofold degenerate, and

$$z_l=\vec{\mathbf{p}}^T\mathbf{T}\mathbf{S}(l)\mathbf{T}^{-1}\vec{\mathbf{1}}. \tag{31}$$

Here, $\mathbf{S}(l)$ is the matrix with elements $\mathbf{S}_{i,j}(l)=\delta_{i,l}\delta_{j,l}$, i.e., with all elements equal to zero, except $S_{l,l}(l)$ which is equal to unity.

From Eqs. (30), (4), and (5) it follows that the spectrum consists of a superposition of absorption peaks with the homogeneous line shape (6), with center frequencies shifted from ω'_{LVM} by the imaginary parts of λ_l, widths given by the real parts of λ_l, relative intensities $\mathrm{Re}[z_l]$, and asymmetries given by $a_l\equiv \mathrm{Im}[z_l]/\mathrm{Re}[z_l]$. At low temperatures ($k_BT \lesssim \hbar\omega'_e$), the theoretical expression for the spectrum simplifies significantly, because only one of the terms, say $l=0$, has appreciable intensity. In this limit, the spectrum can therefore be approximated by a single line of the type

$$I_{|0\rangle\rightarrow|1\rangle}(\omega)\propto \mathrm{Re}(z_0)\left[\frac{(2T_1)^{-1}+|\mathrm{Re}(\lambda_0)|}{\{\omega-[\omega'_{LVM}-\mathrm{Im}(\lambda_0)]\}^2+[(2T_1)^{-1}+|\mathrm{Re}(\lambda_0)|]^2}\right.$$
$$\left.-a_0\frac{\omega-[\omega'_{LVM}-\mathrm{Im}(\lambda_0)]}{\{\omega-[\omega'_{LVM}-\mathrm{Im}(\lambda_0)]\}^2+[(2T_1)^{-1}+|\mathrm{Re}(\lambda_0)|]^2}\right]. \tag{32}$$

Notice, that the broadening due to the lifetime T_1 has been included in this expression by multiplying Eq. (30) with Eq. (3) before calculating the Fourier transform. Also, we have used the fact that the real part of λ_0 is negative, i.e., $|\mathrm{Re}(\lambda_0)|=-\mathrm{Re}(\lambda_0)$, to obtain this expression.

2. Comparison with the experimental temperature dependence of $\mathbf{H}_{BC}^{(+)}$

Having generalized the exchange model for vibrational dephasing to higher temperatures and twofold degenerate exchange modes, we can now compare the model predictions with the experimental data obtained for the 1998-cm^{-1} line of $\mathrm{H}_{BC}^{(+)}$. The solid curves in Figs. 3(a,c) and 3(b,d) show the frequency shift $|\mathrm{Im}(\lambda_0)|/(2\pi c)$ and the line broadening $|2\,\mathrm{Re}(\lambda_0)|/(2\pi c)$ as a function of T and $1/T$. The curves were calculated with the exchange model, assuming a *nondegenerate* exchange mode and using the best-fit parameters for $\mathrm{H}_{BC}^{(+)}$ given in Table II. The parameters were obtained by a combined fit of $\ln[|\mathrm{Im}(\lambda_0)|/(2\pi c)]$ and $\ln[|2\,\mathrm{Re}(\lambda_0)|/(2\pi c)]$ to the natural logarithm of the experimental data in the temperature range 25-80 K. The number of exchange-mode levels, $n_e^{max}+1$, was chosen sufficiently large that the model predictions were independent of n_e^{max}. We note that the line shape of the extended model converges towards the results of Harris and co-workers given by Eqs. (11) and (12) for $T\rightarrow 0$, as expected.

The dotted curves in Figs. 3(a–d) show the best-fit shift and broadening obtained with the extended exchange model in the case of a twofold degenerate exchange mode. The dotted and full curves are nearly indistinguishable, which shows that the degeneracy of the exchange mode cannot be determined from the shift and broadening alone. As shown in Table II, the best-fit parameters $\delta\omega$ and τ obtained for a nondegenerate and twofold degenerate exchange mode differ by a factor of two, whereas ω'_e is independent of the degeneracy. Consequently, $\delta\omega$ and τ cannot be determined accurately unless the degeneracy of the exchange mode can be determined by some other means.

TABLE II. Exchange model parameters obtained by a combined least-squares fit of $\ln[|\mathrm{Im}(\lambda_0)|/(2\pi c)]$ and $\ln[|2\,\mathrm{Re}(\lambda_0)|/(2\pi c)]$ of the extended exchange model to the experimental shift $\ln|\Delta\omega|$ and broadening $\ln\Delta\Gamma_2^*$ of $\mathrm{H}_{BC}^{(+)}$ and $\mathrm{D}_{BC}^{(+)}$ in the temperature range 25–80 K. The parameters in the columns denoted *A* mode (*E* mode) were obtained assuming a nondegenerate (twofold degenerate) exchange mode. The error bars on the parameters were obtained using the procedure described in Ref. 45.

	$\mathrm{H}_{BC}^{(+)}$ *A* mode	$\mathrm{H}_{BC}^{(+)}$ *E* mode	$\mathrm{D}_{BC}^{(+)}$ *A* mode	$\mathrm{D}_{BC}^{(+)}$ *E* mode
ω'_e (cm^{-1})	114 ± 3	114 ± 3	112 ± 2	112 ± 2
$\delta\omega$ (cm^{-1})	-44 ± 8	-22 ± 4	-46 ± 4	-23 ± 2
τ (ps)	0.14 ± 0.03	0.28 ± 0.06	0.18 ± 0.02	0.37 ± 0.04

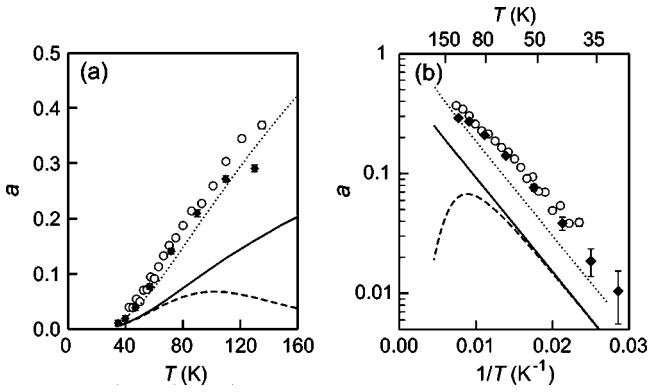

FIG. 5. (a) Plot of the asymmetry parameter a of the 1998-cm^{-1} line as a function of T. (b) Semilogarithmic plot of a vs. $1/T$. The data indicated by diamonds (♦) were obtained with sample SiH 1 (SiH 2). The solid (dotted) curves represent the T dependence of the asymmetry parameter obtained from the exchange model with a nondegenerate (twofold degenerate) exchange mode using the parameters given in Table II. The dashed curves were obtained with the two-level exchange model.

Both the solid and dotted curves in Figs. 3(a–d) are in excellent agreement with the data for $T<80$ K. However, at higher temperatures the absolute deviations are quite substantial. There are a number of possible explanations for these deviations: First, it cannot be ruled out that the stretch mode of $H_{BC}^{(+)}$ is coupled anharmonically to another exchange mode with larger ω_e', which starts to get thermally populated around 100 K. Second, we have assumed that the exchange-mode levels are equally spaced. However, anharmonicity quite generally causes the level spacing to decrease with increasing quantum number, which may affect the temperature dependence of the line shape. Finally, the thermal excitation and deexcitation of the exchange mode was described within the Markovian approximation, which requires that the mean time between thermal excitation events for the exchange mode (inverse excitation rate) be much larger than the correlation time of the phonon bath. With the parameters given in Table II, the inverse rate of $|n_e=0\rangle \rightarrow |n_e=1\rangle$ excitations is ~ 1 ps at ~ 100 K. This is quite similar to the lifetimes of acoustic phonons in Si, obtained from neutron scattering measurements,[46] which can be taken as a measure of the phonon correlation time. Thus, phonon correlation effects may be important at ~ 100 K and above.

In addition to exhibiting a large shift in frequency and increase in linewidth, the 1998-cm^{-1} line becomes significantly asymmetric at elevated temperatures. Figures 5(a,b) show the amplitude of the asymmetric term of the line shape function a as a function of T and $1/T$. The parameters a were obtained by fitting Eq. (6) to the experimental absorbance profiles. The solid and dotted curves in the figure are the temperature dependencies of the asymmetry parameter a_0 obtained with the extended exchange model for, respectively, a nondegenerate and twofold degenerate exchange mode. The curves were calculated from the model parameters in Table II, which were obtained by fitting the model predictions to the shift and broadening of the 1998-cm^{-1} line. Consequently, *no additional fitting has been performed* to obtain the curves in Figs. 5(a,b). Both the experimental and theoretical temperature dependencies of the asymmetry parameters exhibit Arrhenius-type behavior. The two simulated curves are nearly parallel with the experimental data, which shows that the exchange model predicts the activation energy quite accurately. In fact, the activation energy predicted by the model is $\hbar\omega_e'$, identical to those of the frequency shift and the line broadening. More interestingly, the solid and dotted curves are displaced from each other, which shows that the preexponential factor is strongly dependent on the degeneracy of the exchange mode. In fact, the asymmetry parameter with a twofold degenerate exchange mode is exactly twice as large as with a nondegenerate exchange mode. According to Fig. 5(a), the dotted curve is in much better agreement with the data than the full curve, and we therefore conclude that the exchange mode is twofold degenerate.

3. Comparison with the two-level exchange model

The temperature dependencies of the model of Harris and co-workers given in Eqs. (11) and (12) were derived under the assumption $k_BT \ll \hbar\omega_e'$. More specifically, they were based on two low-T assumptions: First, only the two lowest levels of the exchange mode were taken into account ($n_e^{max}=1$), and, second, the frequency shift and broadening were expanded to first order in the quantity $\eta=\exp[-\hbar\omega_e'/k_BT]$ about $\eta=0$. This expansion is invalid at elevated temperatures, and the result of extending the exchange model to include levels with $n_e>1$ should therefore be evaluated by comparison with the predictions of the model of Harris and co-workers without the low-T Taylor expansion. This can be done using the extended exchange model limited to only two exchange-mode levels, which is referred to as *the two-level exchange model* in the remainder of this paper.[47] The theoretical frequency shift and line broadening of the two-level exchange model are shown as the dashed curves in Figs. 3(a–d). The line broadening has a maximum at ~ 150 K, in disagreement with the experimental data, which exhibit a monotonic, superexponential increase up to this temperature. In contrast, the two-level exchange model reproduces the frequency shift quite accurately. The dashed curves in Figs. 5(a,b) show the T dependence of the asymmetry parameter a_0 obtained from the two-level exchange model. As in the case of the line broadening, the asymmetry parameter of the two-level exchange model has a maximum at ~ 100 K in contrast to the experimental observations.

4. Isotope substitution

The excellent agreement between the measured temperature dependence of the 1998-cm^{-1} line and the theoretical predictions of the extended exchange model strongly suggests that the dephasing of the stretch mode of $H_{BC}^{(+)}$ in Si is caused by anharmonic coupling with a twofold degenerate, vibrational mode with frequency $\omega_e'=114$ cm^{-1}. Insight into the nature of the exchange mode can be obtained by isotope substitution experiments. If, for instance, the exchange mode corresponds to the H-related bend mode of $H_{BC}^{(+)}$, then substitution of H with D is expected to change

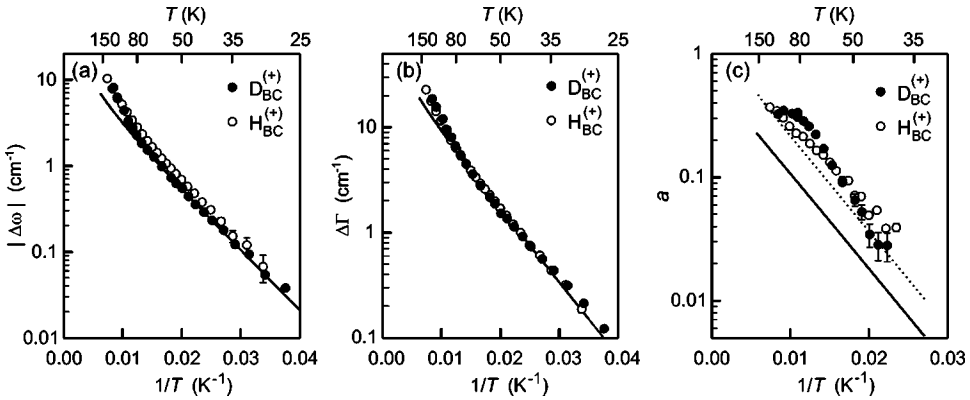

FIG. 6. Comparison of the T dependencies of the 1998-cm^{-1} line of $H_{BC}^{(+)}$ (○) and the 1449-cm^{-1} line of $D_{BC}^{(+)}$ (●). The two data sets were obtained with the same experimental setup (samples SiH 2 and SiD described in Table I) in order to minimize systematic errors on the measured temperatures. The linewidth data shown in (b) have not been corrected for the lifetime contribution to the T dependence. The solid and dotted curves represent the best fit of the exchange model to the SiD data for, respectively, a nondegenerate and a twofold degenerate exchange mode. The curves were generated with the parameters listed in Table II.

the frequency of the exchange mode by a factor $\sim\sqrt{2}$. In contrast, no isotopic shift of ω_e' is expected if the exchange mode primarily involves vibration of Si atoms. To investigate if H is directly involved in the exchange mode, the absorption line shape of the stretch mode of $D_{BC}^{(+)}$ at 1449 cm^{-1} was measured as a function of temperature. Figures 6(a–c) show semilogarithmic plots of the shift, broadening, and asymmetry parameter of the 1449-cm^{-1} line as a function of $1/T$. For comparison, the experimental data obtained for the 1998-cm^{-1} line of $H_{BC}^{(+)}$ with the same cryostat are shown in the same figures. The temperature dependence of the lifetime (T_1) contribution to the width of the 1449-cm^{-1} line has not been measured directly, and the $D_{BC}^{(+)}$ and $H_{BC}^{(+)}$ data have therefore not been corrected for the lifetime contribution in Fig. 6(b). As shown in Fig. 6(b), the increase in linewidth of the 1449-cm^{-1} line associated with $D_{BC}^{(+)}$ coincides with that of $H_{BC}^{(+)}$ at all temperatures in the range 25–130 K. In contrast, the frequency shifts of the two lines differ slightly [see Fig. 6(a)], the frequency shift of the 1449-cm^{-1} line being consistently smaller than that of the 1998-cm^{-1} line in the temperature interval 25–80 K. At higher temperatures the shift of the 1449-cm^{-1} line increases faster than the 1998-cm^{-1} line. The asymmetry parameter of $D_{BC}^{(+)}$, shown in Fig. 6(c), essentially has the same temperature dependence as that of $H_{BC}^{(+)}$, except that it has an oscillatory structure superimposed on the exponential behavior. We believe that this structure is an experimental artifact caused by the fact that the 1449-cm^{-1} line is located close to the edge of the three-phonon absorption band of the Si lattice, which makes baseline correction difficult. The solid (dotted) lines in Figs. 6(a–c) correspond to the line shape parameters obtained with the extended exchange model and the best-fit parameters of $D_{BC}^{(+)}$ given in Table II assuming the exchange mode to be nondegenerate (twofold degenerate). As in the case of $H_{BC}^{(+)}$, the asymmetry for a twofold degenerate exchange mode is in significantly better agreement with the $D_{BC}^{(+)}$ data than the asymmetry of a non-degenerate exchange mode. According to Table II, ω_e' does not shift when D is substituted for H. Consequently, there is no evidence that the exchange mode corresponds to the H-related bending mode of $H_{BC}^{(+)}$.

5. Exact line shape of the exchange model

Although the line shape function (32) represents the experimental line shapes very well at all temperatures, it is an approximation—even within the extended exchange model. It is therefore important to check the validity of the approximation by comparing the result of Eq. (32) with the exact spectrum obtained with the same parameters.

To derive the exact absorption spectrum, we start out combining Eqs. (1) and (29):

$$I_{|0\rangle\rightarrow|1\rangle}(\omega)\propto\vec{\mathbf{p}}^T\mathbf{T}\int_{-\infty}^{\infty}\exp[\mathbf{K}t]dt\ \mathbf{T}^{-1}\vec{\mathbf{1}},$$

where $\mathbf{K}\equiv i(\omega-\omega_{LVM}')\mathbf{I}+\mathbf{\Lambda}-\mathbf{I}(2T_1)^{-1}$. Performing the time integral yields[35]

$$I_{|0\rangle\rightarrow|1\rangle}(\omega)\propto\vec{\mathbf{p}}^T[\mathbf{T}\mathbf{K}^{-1}\mathbf{T}^{-1}+\mathbf{T}^*(\mathbf{K}^*)^{-1}(\mathbf{T}^{-1})^*]\vec{\mathbf{1}},$$

which can be expressed as

$$I_{|0\rangle\rightarrow|1\rangle}(\omega)\propto\mathrm{Im}[\vec{\mathbf{p}}^T\mathbf{A}^{-1}\vec{\mathbf{1}}], \tag{33}$$

where $\mathbf{A}\equiv-i\mathbf{T}\mathbf{K}\,\mathbf{T}^{-1}=(\omega-\omega_{LVM}')\mathbf{I}-\boldsymbol{\delta\omega}-i[\mathbf{W}^T-(2T_1)^{-1}\mathbf{I}]$. Equation (33) is equivalent to the expressions obtained previously by Persson and co-workers[44] and Shelby and co-workers[32] by significantly different methods, except that they did not explicitly take into account the lifetime (T_1) contribution to the line shape. Figure 7 compares the approximated and exact line shapes of the 1998-cm^{-1} line at $T=135$ K obtained from Eqs. (32) and (33) with the best-fit model parameters given in Table II in the case of a nondegenerate exchange mode, and with an assumed lifetime of $T_1=4$ ps. The two spectra are nearly identical, which justifies our use of the approximated function (32) in the analysis.

An alternative expression for the exact line shape, which is completely equivalent to Eq. (33), can be obtained by

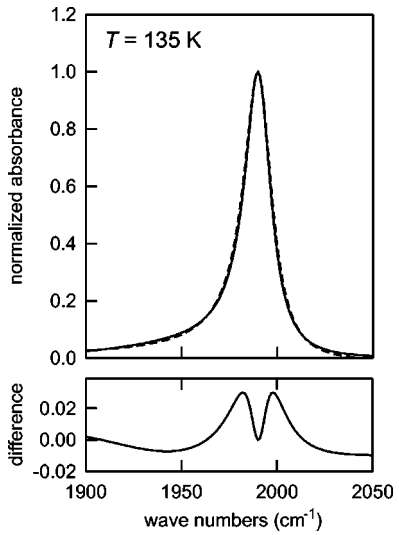

FIG. 7. Exact and approximated line shapes of the exchange model. The solid curve shows the exact line shape obtained from Eq. (33) assuming a nondegenerate exchange mode, and using the $H_{BC}^{(+)}$ parameters given in Table II. The dashed curve is the approximated line shape obtained from Eq. (32) with the same parameters. The bottom graph shows the difference between the two line shapes.

Fourier transformation of Eq. (30). This formulation gives the spectrum as a sum of l_{max} functions of the type in Eq. (32). The approximated line shape corresponds to neglecting all terms in this sum except the one with nonvanishing amplitude $\mathrm{Re}(z_l)$ in the limit $T\rightarrow 0$. The other terms in the sum give rise to sidebands, which may be observed at elevated temperatures. In the case of $H_{BC}^{(+)}$ in Si, these sidebands are very broad because of the very short lifetime $\tau\sim 0.2$ ps of the exchange mode. If, however, the lifetime is longer, say $\tau\sim 1-10$ ps, then the sidebands are relatively narrow and may appear as well-defined peaks in the spectrum. As mentioned in the Introduction, such sidebands have indeed been observed in the case of interstitial oxygen[14] and the Al_{Si}:H and Ga_{Si}:H complexes in Si.[13] We believe that the exchange model, in its present formulation, is able to account quantitatively for the T dependence of the position, width, and intensity of the sidebands observed at elevated temperatures.

VI. DEPHASING DUE TO ANHARMONIC INTERACTIONS WITH LATTICE PHONONS

As demonstrated in the previous section, the T-dependent shift, broadening, and asymmetric shape of the 1998-cm^{-1} line of $H_{BC}^{(+)}$ in Si is in very good agreement with the exchange model, which assumes that dephasing originates from thermal fluctuations in the occupation number of *one particular* low-frequency mode. However, it may seem peculiar that one particular mode should dominate the dephasing dynamics considering that a $\sim$1-cm^3 sample has $\sim 1.5\times 10^{23}$ phonon modes, all of which in principle could contribute. To clarify this issue, this section shows how the exchange model can be generalized to include an arbitrary distribution of independent exchange modes. In particular, dephasing due to lattice phonons is described using the Debye model to represent the phonon distribution. We conclude that thermal fluctuations in the occupation numbers of acoustic phonon modes cannot explain the T-dependent shape of the 1998-cm^{-1} line.

A. Existing phonon dephasing model

The effect of phonons on the spectral shapes of LVM absorption lines was studied theoretically by Elliott and co-workers more than three decades ago.[48] They showed that anharmonic coupling between the LVM and a phonon mode $\vec{\mathbf{k}}_s$ changes the transition frequency by $\Delta\omega_{\vec{\mathbf{k}},s}=\delta\omega_{\vec{\mathbf{k}},s}(\overline{n}_{\vec{\mathbf{k}},s}[T]+\frac{1}{2})$, where $\overline{n}_{\vec{\mathbf{k}},s}[T]=[\exp(\hbar\omega_{\vec{\mathbf{k}},s}/k_BT)-1]^{-1}$ is the mean thermal occupation number of the phonon mode, and the parameter $\delta\omega_{\vec{\mathbf{k}},s}$ represents the strength of the anharmonic coupling. Assuming $\delta\omega_{\vec{\mathbf{k}},s}$ to be proportional to the frequency of the phonon mode $\omega_{\vec{\mathbf{k}},s}$, Elliott and coworkers found

$$\Delta\omega=\sum_{\vec{\mathbf{k}},s}\Delta\omega_{\vec{\mathbf{k}},s}\propto\sum_{\vec{\mathbf{k}},s}\hbar\omega_{\vec{\mathbf{k}},s}(\overline{n}_{\vec{\mathbf{k}},s}+\tfrac{1}{2})=U(T),$$

i.e., that the frequency shift is proportional to the mean vibrational energy $U(T)$ of the lattice. If the Debye model is used to represent the phonon modes, then the temperature dependence takes the form

$$\Delta\omega[T]=C_{\Delta\omega}\int_0^1 x^3\overline{n}[x,T]dx, \tag{34}$$

where $\overline{n}[x,T]\equiv\{\exp[(\theta_D/T)x]-1\}^{-1}$, $C_{\Delta\omega}$ is a constant, and θ_D is the Debye temperature. Furthermore, Elliott and coworkers assumed the width of the absorption line to be proportional to the sum of the rates for exchange processes of the type $|n_{LVM};n_{\vec{\mathbf{k}},s},n_{\vec{\mathbf{k}}',s'}\rangle\rightarrow|n_{LVM};n_{\vec{\mathbf{k}},s}\pm 1,n_{\vec{\mathbf{k}}',s'}\mp 1\rangle$, which exchange one vibrational quantum between the phonon modes $\vec{\mathbf{k}}_s$ and $\vec{\mathbf{k}}'_{s'}$ and conserve the LVM occupation number. In the Debye approximation the T dependence of the linewidth takes the form

$$\Delta\Gamma[T]=C_{\Delta\Gamma}\int_0^1 x^6\overline{n}[x,T](\overline{n}[x,T]+1)dx. \tag{35}$$

Equation (35) has also been derived independently by McCumber and Sturge.[49]

Expressions (34) and (35) have previously been used to analyze the T dependencies of the line shapes of the Zn_{Ga}:H and Be_{Ga}:H complexes in GaP,[50] and the S_{As}:H and Te_{As}:H complexes in GaAs.[51] In both cases, the theoretical expressions represented the data well. We have also fitted Eqs. (34) and (35) to the shift and broadening of the 1998-cm^{-1} line of $H_{BC}^{(+)}$ in Si, and found the fit to be in excellent agreement with the data at all temperatures. It is therefore appropriate to look into dephasing by lattice phonons in more detail.

B. Dephasing dynamics due to phonon coupling

The theory of Elliott and co-workers described above does not take the dynamic nature of the dephasing processes

into account, but simply assumes the frequency shift to be given by the equilibrium population of the phonon modes. Moreover, the theory does not correlate the magnitude of the frequency shift and line broadening, nor does it account for the actual shape of the absorption line. Thus, the theory has to be extended to treat the shift, broadening, and asymmetry in the same footing, in order to be a viable alternative to the exchange model.

The exchange model is quite easily extended from one to an arbitrary number of exchange modes, provided that contributions of the modes to the dephasing of the LVM can be treated independently. More specifically, we assume that the dipole-dipole correlation function takes the form

$$\langle \mu_{01}(0)\mu_{01}^{*}(t)\rangle \propto \exp\left[-i\omega_{LVM}t-\frac{t}{2T_1}\right]\prod_{\vec{\mathbf{k}},s}\varphi_{\vec{\mathbf{k}},s}(t), \tag{36}$$

where the phase relaxation function $\varphi_{01}^{T_2^*}(t)$ of Eq. (5) has been replaced by a product of functions of the type

$$\varphi_{\vec{\mathbf{k}},s}(t)=z_{\vec{\mathbf{k}},s}\exp[\lambda_{\vec{\mathbf{k}},s}t], \tag{37}$$

where $\varphi_{\vec{\mathbf{k}},s}(t)$ is the phase relaxation function due to the mode $\vec{\mathbf{k}}_s$. The variable $\lambda_{\vec{\mathbf{k}},s}$ is the eigenvalue obtained from the exchange model, whereas $z_{\vec{\mathbf{k}},s}$ is the complex amplitude given by Eq. (31). In order to calculate $\lambda_{\vec{\mathbf{k}},s}$ and $z_{\vec{\mathbf{k}},s}$, the exchange-mode parameters $\delta\omega_{\vec{\mathbf{k}},s}$, $\tau_{\vec{\mathbf{k}},s}$, and $\omega_{\vec{\mathbf{k}},s}$ have to specified for each exchange mode. It should be noted that, although we choose to specify the exchange modes by vectors $\vec{\mathbf{k}}$ and branch indices s, most of the theory developed in this section is nonspecific to the type of exchange modes involved, and would therefore apply equally well to exchange modes other than phonons. From Eqs. (1), (36), and (37) it immediately follows that the absorption line shape takes the form of Eq. (6), where the lineshift is given by

$$\Delta\omega=-\sum_{\vec{\mathbf{k}},s}\mathrm{Im}[\lambda_{\vec{\mathbf{k}},s}],$$

the increase in Lorentzian FWHM by

$$\Delta\Gamma=-\sum_{\vec{\mathbf{k}},s}2\,\mathrm{Re}[\lambda_{\vec{\mathbf{k}},s}],$$

and the asymmetry parameter by

$$a=\mathrm{Im}\left[\prod_{\vec{\mathbf{k}},s}z_{\vec{\mathbf{k}},s}\right]\Big/\,\mathrm{Re}\left[\prod_{\vec{\mathbf{k}},s}z_{\vec{\mathbf{k}},s}\right]$$

$$\approx\left(\prod_{\vec{\mathbf{k}},s}\mathrm{Re}[z_{\vec{\mathbf{k}},s}]\right)\sum_{\vec{\mathbf{k}},s}\frac{\mathrm{Im}[z_{\vec{\mathbf{k}},s}]}{\mathrm{Re}[z_{\vec{\mathbf{k}},s}]}.$$

The last relation holds provided that $\mathrm{Im}[z_{\vec{\mathbf{k}},s}]\ll\mathrm{Re}[z_{\vec{\mathbf{k}},s}]$ for all exchange modes, which is the case for coupling to lattice phonons as we will demonstrate later.

If a large number of phonon modes N, $N\gg1$, are assumed to contribute significantly to the dephasing of the LVM, then each mode is coupled weakly to the LVM, and their contribution to the T dependence can be described with the weak-coupling theory of Persson and co-workers.[41] The frequency shift is then given by

$$\Delta\omega[T]=\sum_{\vec{\mathbf{k}},s}\delta\omega_{\vec{\mathbf{k}},s}\bar{n}_{\vec{\mathbf{k}},s}[T]$$

and the linewidth by

$$\Delta\Gamma[T]=\sum_{\vec{\mathbf{k}},s}2\,\delta\omega_{\vec{\mathbf{k}},s}^{2}\tau_{\vec{\mathbf{k}},s}\bar{n}_{\vec{\mathbf{k}},s}[T](\bar{n}_{\vec{\mathbf{k}},s}[T]+1).$$

Similarly, the T dependence of the asymmetry parameter is[52]

$$a[T]=\sum_{\mathbf{k},s}2(\delta\omega_{\vec{\mathbf{k}},s}\tau_{\vec{\mathbf{k}},s})^{3}\bar{n}_{\vec{\mathbf{k}},s}[T](\bar{n}_{\vec{\mathbf{k}},s}[T]+1)\times(2\bar{n}_{\vec{\mathbf{k}},s}[T]+1). \tag{38}$$

The summations over the phonon modes can be performed explicitly if the phonons bands are approximated by the Debye model. With the additional assumptions $\delta\omega_{\vec{\mathbf{k}},s}=\delta\omega_D(\omega_{\vec{\mathbf{k}},s}/\omega_D)$ and $\tau_{\vec{\mathbf{k}},s}=\tau_D(\omega_{\vec{\mathbf{k}},s}/\omega_D)^2$, where $\omega_D=k_B\theta_D/\hbar$ is the Debye frequency, the results are identical to the T dependencies (34) and (35) obtained by Elliott and co-workers, except that the prefactors now are given in terms of the coupling strength $\delta\omega_D$ and the lifetime τ_D at the Debye frequency as $C_{\Delta\omega}=9\,\delta\omega_D N$ and $C_{\Delta\Gamma}=18\delta\omega_D^2\tau_D N$. The integral appearing in expression (35) for the broadening is always less than the one in the expression (34) for the shift for the same θ_D, and the ratio between the line broadening and frequency shift is therefore less than $2\,\delta\omega_D\tau_D$ at all temperatures. However, $\delta\omega_D\tau_D\sim1/N\ll1$ and anharmonic coupling of the LVM to a large number of phonon modes can therefore not give rise to line shifts and broadening of similar magnitude. Similarly, it follows from Eq. (38) that the asymmetry parameter is of the order $(1/N)^2$. Thus, the asymmetry of the line shape is negligible.

To recapitulate, we have argued that anharmonic coupling of the LVM to a large number ($N\gg1$) of exchange modes, e.g., phonons, cannot account for line broadening comparable in magnitude to the line shift, nor for the absorption lines being asymmetric. The reason for this is quite simple: If many exchange modes contribute to the shift, then the contribution from each mode is small, and the LVM and the exchange modes are weakly coupled. In the weak-coupling regime the frequency shift is proportional to the coupling parameter, which scales as $1/N$, and when the contributions from all N exchange modes are added, the total line shift becomes independent of N. However, the line broadening and asymmetry parameter contributions from each mode scale as $1/N^2$ and $1/N^3$, respectively. Therefore, these quantities remain vanishingly small, despite the addition of N contributions, if N is large.

VII. DISCUSSION

To investigate the dependency of the exchange mode on the defect configuration and phonon spectrum of the host material, we now compare the results obtained for $H_{BC}^{(+)}$ in Si

TABLE III. Summary of *T*-dependent line shape studies of H-related stretch modes in semiconductors. The defects denoted X_Y:H in the second column correspond to a H atom forming a complex with an impurity atom *X* located on (or slightly displaced from) a substitutional *Y* site of the semiconductor *YZ* listed in column 1. The V_{In}:H_4 complex consists of four H atoms each bound to one of the four P atoms surrounding an In vacancy in InP. The exchange mode frequencies obtained from the *T* dependencies of the absorption lines and the exchange theories of Persson and co-workers (Ref. 40) and of Harris and co-workers (Refs. 29–31) are listed in the column denoted ω_e'. The columns ''High symmetry phonon'' and ''ω_{phonon}'' list the high-symmetry phonon mode of the host crystal closest to ω_e' and the corresponding phonon frequency. Here, a high-symmetry phonon is defined as a phonon with a *k* vector equal to one of the high-symmetry points Γ, *X*, and *L* in the Brillouin zone, where the phonon density of states is large. The phonon frequencies were obtained from Ref. 56.

Material	Defect	ω_e' (cm^{-1})	High-symmetry phonon	ω_{phonon} (cm^{-1})	Reference
GaAs	C_{As}:H	78	TA_X	79	53
GaAs	Si_{Ga}:H	~ 64	TA_L	62	54
GaAs	S_{As}:H	~ 70	TA_X	79	51
InP	Zn_{In}:H	61	TA_L	55	55
InP	Cd_{In}:H	50	TA_L	55	55
InP	V_{In}:H_4	136	LA_L	166	55
Ge	$H_{BC}^{(+)}$	75 ± 2	TA_X (TA_L)	79 (62)	58
Si	$H_{BC}^{(+)}$	114 ± 3	TA_L	114	This work

with those reported previously for H-related modes in semiconductors. Most studies of the *T*-dependence of absorption line shapes have used the weak-coupling theory of Persson and co-workers,[53–55] whereas Vetterhöffer and Weber[51] found that $|\delta\omega\tau| \sim 1$ for the S_{As}:H and Te_{As}:H complexes in GaAs, and therefore based their analysis on the theory of Harris and co-workers. Although H-related bend modes have been studied also,[51,54] we shall limit the present discussion to H-related stretch modes, the results of which are summarized in Table III. Since the parameters $\delta\omega$ and τ are unreliable unless the degeneracy of the exchange modes are known, only the values of ω_e' are listed in the table.

Table III also contains results for the stretch mode of $H_{BC}^{(+)}$ in Ge, which was identified recently by *in situ* infrared spectroscopy.[57] The line shape studies of $H_{BC}^{(+)}$ in Ge were performed using the same approach as in the present paper.[58] The 1794-cm^{-1} line of $H_{BC}^{(+)}$ in Ge was found to exhibit Arrhenius-type frequency shifts, line broadening, and asymmetry parameters, all of which were characterized by an activation energy $\omega_e' = 75\pm 2\ \mathrm{cm}^{-1}$. The magnitude of the asymmetry parameter was in good agreement with the exchange model provided that the exchange mode was assumed to be twofold degenerate. Consequently, the *T* dependencies of the stretch modes of $H_{BC}^{(+)}$ in Si and Ge are very similar, as one might expect for defects with the same structure.

All the exchange modes listed in Table III are located within the acoustic phonon branches of the pertinent crystal lattices. Most of the modes nearly coincide with TA phonon modes at either the *X* or the *L* point of the Brillouin zone, where the phonon density of states is large, which led some of the authors to assign the exchange modes to such high-symmetry phonons.[53,55] According to Table III, the exchange mode of $H_{BC}^{(+)}$ in Si coincides with TA_L phonons in Si. However, we believe that this coincidence is accidental and instead assign the exchange mode to a pseudolocalized mode (PLM) associated with the $H_{BC}^{(+)}$ defect. There are several reasons for doing so: First, we do not see any reason why the stretch mode of the defect should couple preferentially to any particular phonon mode. If coupled to phonons, we would therefore expect dephasing of the stretch mode to be governed by coupling to a wide distribution of modes. However, according to the discussion in Sec. VI B, dephasing by anharmonic coupling to lattice phonons cannot simultaneously account for the shift, broadening, and asymmetry of the 1998-cm^{-1} line. Second, the exchange modes of $H_{BC}^{(+)}$ in Si and Ge are located differently relative to the phonon bands of the two materials (see Table III). Since $H_{BC}^{(+)}$ has the same structure in Si and Ge, we expect the relative strengths of the anharmonic coupling between the stretch mode and the low-frequency modes to be the same in both materials. Consequently, the stretch mode of $H_{BC}^{(+)}$ should couple to the same type of exchange mode in the two materials, in conflict with the exchange mode being a TA_L phonon in Si but not in Ge. Finally, the *T* dependence of the Al_{Si}:H complex in Si, studied by Stavola and co-workers,[13] is completely consistent with the H-related stretch modes of this complex being coupled to an exchange mode with $\omega_e' = 78\ \mathrm{cm}^{-1}$. In contrast to $H_{BC}^{(+)}$, this exchange mode shifts down in frequency by a factor $\sim\sqrt{2}$ when D is substituted for H, which identifies it as the H-related bending mode of the complex.[59] The structure of the Al_{Si}:H complex is very similar to that of $H_{BC}^{(+)}$. In both cases, H is located at the bond-center site, and the nearest-neighbor atoms relax substantially to accommodate the H atom. The fact that the *T* dependence of the stretch mode of Al_{Si}:H is determined by anharmonic coupling to the bending mode of the complex, which is resonant with the phonon bands, demonstrates that it indeed is possible for a single PLM to determines the dephasing dynamics of a stretching mode. Hence, it strongly supports our assignment of the 114-cm^{-1} exchange mode to a PLM associated with $H_{BC}^{(+)}$.

PLM's are vibrational modes that, despite being resonant with the phonon continuum, are confined to the vicinity of the defect. Relatively little is known about PLM's because they generally are difficult to study experimentally and theoretically. H-related PLM's, like the bending mode of Al_{Si}:H, may exist if the H vibration is coupled weakly to the vibrational motion of the surrounding Si atoms. Moreover, Si-related PLM's may exist if the distortion of the lattice around the defect is sufficiently large.[1] Since Si-related PLM's primarily involve Si atoms, they will not exhibit isotopic shifts when D is substituted for H. When a proton is placed at the center of a Si–Si bond to form $H_{BC}^{(+)}$, the two Si atoms move apart by a distance corresponding to a $\sim 40\%$ increase in the Si–Si bond length.[6] Because of this very large relaxation, $H_{BC}^{(+)}$ in Si is likely to have Si-related PLM's.

The vibrational modes of $H_{BC}^{(+)}$ can be illustrated with the

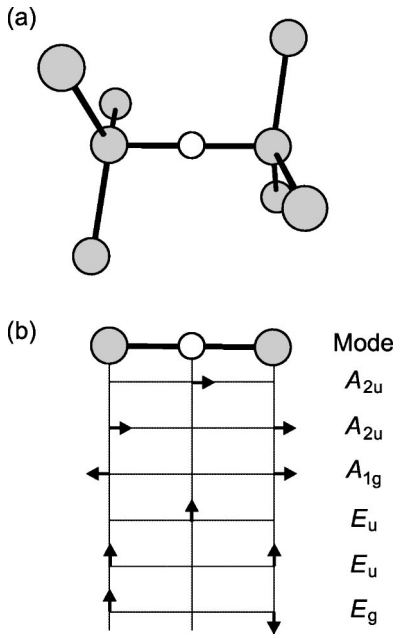

FIG. 8. (a) Structure of $H_{BC}^{(+)}$ in Si and Ge. The white circle represents the H atom, whereas the gray circles are Si or Ge. (b) Normal modes associated with $H_{BC}^{(+)}$ in Si and Ge. The normal modes are highly simplified to better illustrate the basic features of the modes: Only vibration of the H atom and its two nearest neighbors are considered. Moreover, the vibrational amplitudes of the host atoms associated the H-related modes and the amplitudes of the H atom for the Si-related modes are not shown. Finally, the vibrational amplitudes are not drawn to scale.

simplified model system shown in Fig. 8(a), which consists of a H atom surrounded by two shells of Si atoms, containing, respectively, two and six atoms. The model system has a D_{3d} point group like $H_{BC}^{(+)}$. For simplicity, we keep the six outermost Si atoms fixed, which leaves nine vibrational degrees of freedom. Displacement of the three atoms parallel to the trigonal axis gives rise to three nondegenerate modes; one mode with A_{2u} symmetry, which primarily involves the H atom (the H-related stretch mode), and two Si-related modes with A_{1g} and A_{2u} symmetry [see Fig. 8(b)]. Vibration perpendicular to the trigonal axis gives rise to three twofold degenerate modes, two with E_u symmetry and one with E_g symmetry. If the coupling matrix element between the two E_u modes is much less than their frequency difference, then one of the modes can be associated with the vibration of H perpendicular to the trigonal axis (the H-related bend mode), whereas the other mode primarily involves displacement of the two Si atoms in the same direction, as shown in Fig. 8(b). Finally, the E_g mode corresponds to the two Si atoms vibrating in opposition perpendicularly to the trigonal axis. In the previous sections we have presented strong evidence that the exchange mode of $H_{BC}^{(+)}$ in Si is twofold degenerate, and the three E modes described above are therefore the best exchange mode candidates. Furthermore, the absence of isotopic shift for ω_e' suggests that the exchange mode is *not* H related, and we therefore ascribe it to the Si related E_g or E_u modes in Fig. 8(b). This interpretation is consistent with simple geometric considerations. Stretch-mode frequencies are known to be strongly dependent on the bond length. For instance, first-principle calculations of the LVM frequencies of the H_2^* defect in Ge have shown that elongation of the Ge–H bond by 3% caused the stretch mode frequency to decrease by $\sim 250\ \mathrm{cm}^{-1}$.[11] Excitation of the Si-related E_g mode shown in Fig. 8(b) increases the root-mean-square (rms) length of the Si–H–Si bond because the rms distance of the Si atoms from the $\langle 111 \rangle$ axis increases with increasing quantum number of the E_g mode. In contrast, excitation of longitudinal Si-related modes, like the A_{1g} and A_{2u} modes shown in the figure, does not increase the rms Si–H–Si bond length if the Si atoms vibrate symmetrically around their equilibrium positions. Thus, simple geometric considerations are consistent with the stretch mode of $H_{BC}^{(+)}$ being coupled more strongly to transverse Si-related modes than to longitudinal modes and also explain the negative sign of $\delta\omega$.

The preceding discussion of the normal modes of $H_{BC}^{(+)}$ is highly simplified because of the small number of Si atoms included in the model. In reality, the Si-related modes, and possibly also the H-related bend mode, will couple to the vibrational degrees of freedom of the surrounding shells of Si atoms, which will make the normal modes more delocalized than shown in Fig. 8(b). The degree of localization depends on the change in the force constants of the Si–Si bonds in the vicinity of the defect due to the $\sim 40\%$ expansion of the Si–H–Si bond. Such quantities are difficult to estimate, but should be within the reach of first-principles calculations. Our studies of the vibrational dynamics of $H_{BC}^{(+)}$ reported here and in Ref. 16 strongly suggest that PLM's play an important role in pure dephasing and population relaxation processes of LVM's. However, a better theoretical understanding of PLM's is required to fully understand the nature of dephasing and population relaxation processes of point defects in solids.

VIII. CONCLUSION

In conclusion, the shape of the fundamental absorption line of the H-related stretch mode of $H_{BC}^{(+)}$ in Si was measured with *in situ* infrared spectroscopy. The line exhibits an Arrhenius-type down-shift in frequency and increase in linewidth with the same activation energy $\hbar\omega_e'$, as predicted by theoretical dephasing models of Harris and co-workers and of Persson and co-workers. In addition, the absorption line becomes significantly asymmetric at elevated temperatures, which cannot be explained within these dephasing theories. To explain the experimental data, the model of Harris and co-workers was extended beyond the low-T limit, and the theory was generalized to include a twofold degenerate exchange mode. It was shown that the shift, broadening, and asymmetry predicted by the exchange model depends strongly on the degeneracy of the exchange mode and that the parameters $\delta\omega$ and τ obtained from the model therefore are unreliable unless the degeneracy of the mode is known.

The T-dependence predicted by the extended exchange model was found to be in excellent agreement with the observations for $H_{BC}^{(+)}$ in Si. In particular, the theoretical line shape function represented the asymmetric shape of the

1998-cm^{-1} line very well at all temperatures. The best-fit frequency shifts and linewidths were in excellent agreement with the experimental data up to ~100 K, irrespective of the degeneracy of the exchange mode. In contrast, the asymmetry parameter was in good agreement with the data only in the case of a twofold degenerate exchange mode. The T dependencies of $H_{BC}^{(+)}$ and $D_{BC}^{(+)}$ are essentially identical, showing that the exchange mode does not correspond to the H-related bend mode of the defect.

The exchange model was generalized from 1 to N exchange modes, where $N \gg 1$, in order to investigate the effect of coupling to many modes. The expressions for the line shift and broadening were consistent with the theory of Elliott and co-workers, but the magnitude of the line broadening predicted by the model was of the order $1/N$ less than the frequency shift. This is inconsistent with the experimental data for $H_{BC}^{(+)}$ in Si, and we therefore conclude that dephasing of the 1998-cm^{-1} mode is not governed by coupling to lattice phonons.

The T-dependent shape of the 1998-cm^{-1} line is in excellent agreement with the exchange model in its present form, which suggests that the dephasing of the H-related stretch mode of $H_{BC}^{(+)}$ is caused by thermal fluctuations in the occupation number of a single, twofold degenerate mode at 114 cm^{-1}. The exchange mode is ascribed to a Si-related pseudolocalized mode associated with $H_{BC}^{(+)}$.

ACKNOWLEDGMENTS

M. Budde and C. Parks Cheney gratefully acknowledge the hospitality of B. Bech Nielsen and the Aarhus Center for Atomic Physics (ACAP) during their stay at the Institute of Physics and Astronomy, Aarhus University, Denmark. We also thank Walter M. Augustyniak for technical support during the experiments at Vanderbilt University. This work was supported by DOE through Grant No. DE-FG02-99ER45781. G. Lüpke gratefully acknowledges the Alexander von Humboldt foundation for financial support.

APPENDIX: FREQUENCY SHIFT DUE TO THERMAL EXPANSION

Frequencies of LVM's are strongly dependent on the length of the bond(s) between the impurity and the atoms of the crystalline host material. Changes to the bond lengths induced by thermal expansion (or compression) of the crystal will therefore generally lead to a temperature dependence of the LVM frequencies. Since this contribution to the T-dependent shift of the absorption line is not included in the exchange model for vibrational dephasing, we need to estimate its magnitude and correct for it, if necessary.

The frequency shift induced by thermal expansion can be calculated once the response of the absorption line on uniaxial stress, the elastic properties of the host material, and its thermal expansion coefficient are known. The stress-induced frequency shift can in the case of a nondegenerate LVM be expressed as[60]

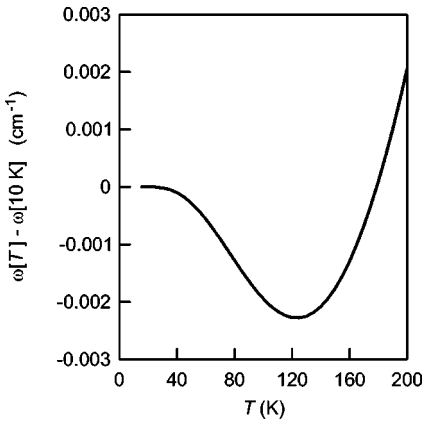

FIG. 9. Frequency shift of the 1998-cm^{-1} line caused by thermal changes to the lattice constant of the Si lattice.

$$\Delta\omega = \sum_{i,j=1}^{3} A_{i,j}\sigma_{i,j}, \tag{A1}$$

where $A_{i,j}$ are the elements of the piezospectroscopic tensor, which can be determined by uniaxial stress experiments, and $\sigma_{i,j}$ are elements of the stress tensor. Thermal expansion is isotropic and therefore results in an isotropic stress tensor with elements

$$\sigma_{i,j}(T) = [C_{11} + 2C_{12}]\frac{a[T] - a[10\mathrm{K}]}{a[10\mathrm{K}]}\delta_{i,j}, \tag{A2}$$

expressed in terms of the second-order elastic moduli of Si, C_{11} and C_{12}, and the fractional change in lattice parameter $(a[T] - a[10\ \mathrm{K}])/a[10\ \mathrm{K}]$ relative to the lattice parameter at $T = 10$ K. With this form of the fractional change in lattice parameter, the frequency shift is calculated relative to the frequency at $T = 10$ K, the lowest temperature at which the absorption spectrum was measured in the present work. Inserting Eq. (A2) into Eq. (A1) yields

$$\omega[T] - \omega[10\mathrm{K}] = 3[C_{11} + 2C_{12}]A_1\frac{a[T] - a[10\mathrm{K}]}{a[10\mathrm{K}]}, \tag{A3}$$

where we have introduced A_1, which is equal to $A_{1,1}$, $A_{2,2}$, and $A_{3,3}$ for an A_{2u} mode of a defect with D_{3d} symmetry like the 1998-cm^{-1} mode of $H_{BC}^{(+)}$.[60]

The fractional change in lattice parameter can be expressed in terms of the linear thermal expansion coefficient $\alpha[T]$ as

$$\frac{a[T] - a[10\mathrm{K}]}{a[10\mathrm{K}]} = \exp\left[\int_{10\mathrm{K}}^{T}\alpha[T]dT\right] - 1. \tag{A4}$$

Using the value $A_1 = 9$ cm^{-1}/GPa for the 1998-cm^{-1} line (Ref. 61), and tabulated values of $\alpha[T]$ (Ref. 62), C_{11}, and C_{12} (Ref. 55) for Si, the frequency shift due to thermal expansion of the Si lattice can be calculated from Eqs. (A3) and (A4). As shown in Fig. 9, the frequency shift is less than 3×10^{-3} cm^{-1} in the temperature range 10–200 K, and thermal expansion therefore contributes negligibly to the frequency shift of the 1998-cm^{-1} line.

*Present address: Division of Engineering and Applied Sciences, Harvard University, Cambridge, MA 02138 and Rowland Institute for Science, Cambridge, MA 02142. Electronic address: budde@fas.harvard.edu

[1] A.S. Barker, Jr. and A.J. Sievers, Rev. Mod. Phys. **47**, Suppl. No. 2, S1 (1975).

[2] *Identification of Defects in Semiconductors: Semiconductors and Semimetals*, edited by M. Stavola (Academic Press, New York, 1999), Vol. 51B, Chap. 3.

[3] *Hydrogen in Semiconductors: Semiconductors and Semimetals*, edited by J.I. Pankove and N.M. Johnson (Academic Press, New York, 1991), Vol. 34.

[4] S.J. Pearton, J.W. Corbett, and M. Stavola, *Hydrogen in Crystalline Semiconductors* (Springer-Verlag, Berlin, 1992).

[5] *Hydrogen in Semiconductors II: Semiconductors and Semimetals*, edited by N.H. Nickel (Academic Press, New York, 1999), Vol. 61.

[6] S.K. Estreicher, Mater. Sci. Eng., R. **14**, 319 (1995).

[7] See, e.g., Refs. 3 and 4, and references therein.

[8] S.J. Uftring, M. Stavola, P.M. Williams, and G.D. Watkins, Phys. Rev. B **51**, 9612 (1995).

[9] B. Bech Nielsen, L. Hoffmann, and M. Budde, Mater. Sci. Eng. B **36**, 259 (1996); M. Budde, B. Bech Nielsen, P. Leary, J. Goss, R. Jones, P.R. Briddon, S. Öberg, and S.J. Breuer, Phys. Rev. B **57**, 4397 (1998).

[10] J.D. Holbech, B. Bech Nielsen, R. Jones, P. Sitch, and S. Öberg, Phys. Rev. Lett. **71**, 875 (1993).

[11] M. Budde, B. Bech Nielsen, R. Jones, J. Goss, and S. Öberg, Phys. Rev. B **54**, 5485 (1996).

[12] A.W.R. Leitch, V. Alex, and J. Weber, Phys. Rev. Lett. **81**, 421 (1998); R.E. Pritchard, M.J. Ashwin, J.H. Tucker, and R.C. Newman, Phys. Rev. B **57**, 15 048 (1998); J. Anna Zhou and M. Stavola, Phys. Rev. Lett. **83**, 1351 (1999).

[13] M. Stavola, S.J. Pearton, J. Lopata, and W.C. Dautremont-Smith, Phys. Rev. B **37**, 8313 (1988).

[14] R.C. Newman, Adv. Phys. **18**, 545 (1969); D.R. Bosomworth, W. Hayes, A.R.L. Spray, and G.D. Watkins, Proc. R. Soc. London, Ser. A **317**, 133 (1970).

[15] A. Nitzan and J. Jortner, Mol. Phys. **25**, 713 (1973); A. Nitzan, S. Mukamel, and J. Jortner, J. Chem. Phys. **60**, 3929 (1974).

[16] P. Guyot-Sionnest, P. Dumas, Y.J. Chabal, and G.S. Higashi, Phys. Rev. Lett. **64**, 2156 (1990).

[17] M. Budde, G. Lüpke, C. Parks Cheney, N.H. Tolk, and L.C. Feldman, Phys. Rev. Lett. **85**, 1452 (2000).

[18] B. Bech Nielsen, in *Oxygen, Carbon, Hydrogen and Nitrogen in Crystalline Silicon*, edited by J.C. Mikkelsen, Jr., S.J. Pearton, J.W. Corbett, and S.J. Pennycook, MRS Symposia Proceedings No. 50 (Materials Research Society, Pittsburgh, 1986), p. 487; B. Bech Nielsen, Phys. Rev. B **37**, 6353 (1988).

[19] Y.V. Gorelkinskii and N.N. Nevinnyi, Pis'ma Zh. Tekh. Fiz. **13**, 105 (1987) [Sov. Tech. Phys. Lett. **13**, 45 (1987)]; Y.V. Gorelkinskii in *Hydrogen in Semiconductors: Semiconductors and Semimetals*, Ref. 5, Chap. 3.

[20] B. Bech Nielsen, K. Bonde Nielsen, and J.R. Byberg, in *Defects in Semiconductors 17*, edited by H. Heinrich and W. Jantch, Materials Science Forum No. 143-147 (Trans-Tech, Aedermannsdorf, Switzerland, 1994), p. 909.

[21] K. Irmscher, H. Klose, and K. Maass, J. Phys. C **17**, 6317 (1984).

[22] B. Holm, K. Bonde Nielsen, and B. Bech Nielsen, Phys. Rev. Lett. **66**, 2360 (1991).

[23] K. Bonde Nielsen, B. Bech Nielsen, J. Hansen, E. Andersen, and J.U. Andersen, Phys. Rev. B **60**, 1716 (1999).

[24] H.J. Stein, Phys. Rev. Lett. **43**, 1030 (1979).

[25] S.K. Estreicher, Phys. Rev. B **36**, 9122 (1987).

[26] P. Deák, L.C. Snyder, and J.W. Corbett, Phys. Rev. B **37**, 6887 (1988).

[27] C.G. Van de Walle, P.J.H. Denteneer, Y. Bar Yam, and S.T. Pantelides, Phys. Rev. B **39**, 10 791 (1989).

[28] R. Jones, Physica B **170**, 181 (1991).

[29] K.J. Chang and D.J. Chadi, Phys. Rev. Lett. **62**, 937 (1989).

[30] C.B. Harris, R.M. Shelby, and P.A. Cornelius, Phys. Rev. Lett. **38**, 1415 (1977); S. Marks, P.A. Cornelius, and C.B. Harris, J. Chem. Phys. **73**, 3069 (1980).

[31] C.B. Harris, R.M. Shelby, and P.A. Cornelius, Chem. Phys. Lett. **57**, 8 (1978).

[32] R.M. Shelby, C.B. Harris, and P.A. Cornelius, J. Chem. Phys. **70**, 34 (1979).

[33] P.W. Anderson, J. Phys. Soc. Jpn. **9**, 316 (1954).

[34] R.G. Gordon, in *Advances in Magnetic Resonance*, edited by J.S. Waugh (Academic Press, New York, 1968), Vol. 3.

[35] To obtain this result we have used the relation $\varphi(-t)=\varphi^*(t)$, which is required for the spectral function $I_{|0\rangle\rightarrow|1\rangle}(\omega)$ to be real (Refs. 32 and 33).

[36] H. Ueba, Prog. Surf. Sci. **55**, 115 (1997).

[37] D.D. Dlott, in *Laser Spectroscopy of solids II*, edited by W.M. Yen (Springer-Verlag, Berlin, 1989), Chap. 5.

[38] J.F. Ziegler, J.P. Biersack, and U. Littmark, *The Stopping and Ranges of Ions in Solids* (Pergamon Press, New York, 1985).

[39] The implantation simulation software SRIM can be downloaded free of charge from J.F. Ziegler's home page at http://www.research.ibm.com/ionbeams/home.htm.

[40] To increase the weight of the low-temperature data, $\ln[|\Delta\omega|]$ and $\ln[\Delta\Gamma_2^*]$ were fitted to a linear function of $1/T$.

[41] B.N.J. Persson and R. Ryberg, Phys. Rev. B **32**, 3586 (1985); A. Nitzan and B.N.J. Persson, J. Chem. Phys. **83**, 5610 (1985).

[42] The matrices $\boldsymbol{\mu}$ and $\mathbf{H}$ are the matrix representations of the operators in the basis defined by the states of the normal modes.

[43] The occupation number $n_e[t]$ being a Markovian random function of time means that the probability of $n_e[t]$ to attain a given value n_1 at time t_1, provided that the value was n_2 at time $t_2=t_1-\Delta t$, is independent of the value of $n_e[t]$ at any time earlier than $t_1-\Delta t$. For a more thorough description see Ref. 32 and references therein.

[44] B.N.J. Persson, F.M. Hoffmann, and R. Ryberg, Phys. Rev. B **34**, 2266 (1986).

[45] The error analysis was performed the following way: First, independent linear fits to the data sets $\ln|\Delta\omega|$ vs $1/T$ and $\ln|\Delta\Gamma_2^*|$ vs $1/T$ were performed in the temperature range 25–80 K. The error bar on ω_e', given in Table II, is taken to be twice the standard error on the mean value of the two slopes. The parameters $\delta\omega$ and τ can be expressed in terms of the two preexponential factors of Eqs. (11) and (12). From the two offset parameters (y intercepts) obtained by the linear fits, the parameters $\delta\omega$ and τ and their standard errors can be calculated. The error bars on $\delta\omega$ and τ given in Table II are twice the standard errors on $\delta\omega$ and τ deduced from the two y intercepts. Notice that only the error bars are estimated this way. The values of ω_e', $\delta\omega$, and

τ given in the table were obtained by a combined least-squares analysis of the shift and the broadening.

[46] Nilsson and Nelin measured the bandwidths of phonon modes in Si and Ge by thermal-neutron spectrometry [G. Nilsson and G. Nelin, Phys. Rev. B **3**, 364 (1971); **6**, 3777 (1972)]; The bandwidths of acoustic phonons at ~ 150 cm^{-1} in Si were found to be 0.16 THz at 300 K, which implies that the to phonon lifetimes are larger than 2 ps [*ibid.* **3**, 364 (1971)].

[47] In order to fulfill the principle of detailed balance, the transition probability matrix has to be truncated properly. This is done by letting $W_{n_e^{max},n_e^{max}} = -\frac{1}{\tau} n_e^{max}(\overline{n_e}+1)$ (Ref. 40).

[48] R.J. Elliott, W. Hayes, G.D. Jones, H.F. MacDonald, and C.P. Sennett, Proc. R. Soc. London, Ser. A **289**, 1 (1965).

[49] D.E. McCumber and M.D. Sturge, J. Appl. Phys. **34**, 1682 (1963).

[50] M.D. McCluskey, E.E. Haller, J. Walker, and N.M. Johnson, Phys. Rev. B **52**, 11 859 (1995).

[51] J. Vetterhöffer and J. Weber, Phys. Rev. B **53**, 12 835 (1996).

[52] The expression $a[T]=2(\delta\omega_{\vec{k},s}\tau_{\vec{k},s})^3 n_{\vec{k},s}[T](n_{\vec{k},s}[T]+1)\times(2n_{\vec{k},s}[T]+1)$ for the contribution to the asymmetry parameter from a single exchange mode in the weak-coupling limit has, to our knowledge, not been stated previously. We obtained this expression by calculating a for a wide range of parameters $\delta\omega_{\vec{k},s}$, $\tau_{\vec{k},s}$, and $\omega_{\vec{k},s}$ with the exchange model developed in Sec. V, and then worked backwards to obtain the mathematical expression that reproduced the results. We have not been able to derive the expression analytically.

[53] B. Clerjaud, D. Cote, F. Gendron, W.-S. Hahn, M. Krause, C. Porte, and W. Ulrici, in *Defects in Semiconductors 16*, edited by G. Davies, M. Stavola, and G. DeLeo, Materials Science Forum No. 83–87 (Trans Tech, Aedermannsdorf, 1992), p. 563.

[54] E. Tuncel and H. Sigg, Phys. Rev. B **48**, 5225 (1993).

[55] R. Darwich, B. Pajot, B. Rose, D. Robein, B. Theys, R. Rahbi, C. Porte, and F. Gendron, Phys. Rev. B **48**, 17 776 (1993).

[56] *Semiconductors—Basic Data*, edited by O. Madelung (Springer-Verlag, Berlin, 1996).

[57] M. Budde, B. Bech Nielsen, C. Parks Cheney, N.H. Tolk, and L.C. Feldman, Phys. Rev. Lett. **85**, 2965 (2000).

[58] C. Parks Cheney, M. Budde, N.H. Tolk, and L.C. Feldman (unpublished).

[59] In the case of the Al_{Si}:H complex in Si, a sideband appears at elevated temperatures (Ref. 12). As discussed in Sec. V D 5, such sidebands can be explained by the present formulation of the exchange model. The parameter $\delta\omega$ is approximately given by the splitting between line observed at low T and the side band, and is -39 cm^{-1} for Al_{Si}:H. Also, it is interesting to note that the sideband of Al_{Si}:H is more intense than the low–T line above ~ 100 K. This is only possible if the exchange mode is degenerate, which is consistent with the assignment of the mode to the twofold degenerate H-related bend mode of the Al_{Si}:H complex.

[60] A.A. Kaplyanskii, Opt. Spektrosk. **16**, 329 (1964) [Opt. Spectrosc. **16**, 602 (1964)].

[61] M. Budde and B. Bech Nielsen (unpublished).

[62] K.G. Lyon, G.L. Salinger, C.A. Swenson, and G.K. White, J. Appl. Phys. **48**, 865 (1977).